UNIVERSITÀ
DEGLI STUDI
DI PADOVA

DIPARTIMENTO
DI INGEGNERIA
DELL'INFORMAZIONE

DIPARTIMENTO DI INGEGNERIA DELL'INFORMAZIONE

CORSO DI LAUREA MAGISTRALE IN BIOINGEGNERIA INDUSTRIALE

"Mechanical validation of Digital Anatomy Printed cartilages for personalized healthcare "

Laureando: Gianmarco Dolino

Relatore: Prof. Mattia Veronese

Correlatore: Prof. Paolo Gargiulo

ANNO ACCADEMICO 2022 – 2023

Data di laurea 13/04/2023

Contents

Abstract

One of the main extrinsic risk factors for osteoarthritis (OA) is chondral lesions, which has significant social and economical impacts. OA is a very common illness that can cause debilitating pain and physical function loss. The present work was carried out at Reykjavik University, Iceland, in the frame of the European Project RESTORE, a multidisciplinary project with the purpose of discovery and offer novel solutions for the treatment of chondral lesions and cartilage degeneration. The aim of this study is the mechanical characterization of innovative Polyjet materials provided by Digital Anatomy Printer technology and the validation of an innovative testing setup, designed in order the make the mechanical tests specific for each patient.

To do so, patient specific medical data were processed in order to extract 3-dimensional models that served as a starting point for computational analysis and advanced additive manufacturing. The innovative Polyjet materials utilized in the process were designed in order to mimic the articular cartilage tissue mechanical performance and printed with patient specific morphologies for the femoral cartilage, alongside with femur and tibia. Following the additive manufacturing process, mechanical tests were performed on printed parts and a parallel finite element analysis was carried out in order to compare the results and validate the model.

The mechanical evaluation of the Digital Anatomy Materials was successful, but the validation of the proposed innovative testing setup still has to be completed. However, a first interesting insight of its potential is shown in a comparison of force-displacement curves with the parallel computational model. Another notably result is the reliability of the model to underline the zones subjected to major deformation. This is of interest because it could lead to the prediction of zones where cartilage deterioration is more likely to occur in the presence of osteoarthritis.

In the future, more solutions should be explored, starting from a finer mimicking of native cartilage tissue mechanical performance. The model has the potential to become more and more complete by adding other anatomical parts by steps and at a certain point it could be achievable to obtain a full knee joint model for research purposes.

Introduction

The most diffused form of joint disease worldwide is osteoarthritis (OA). It is one of the most common causes of pain, loss of function, and adult disability in Western countries. By the age of 65, the majority of people have radiographic evidence of OA and this increases even more over 75 years, with 80% of population having symptoms. For istance, in the US it is the second-leading cause of job incapacity for men over 50 and is responsible for more hospital admissions than rheumatoid arthritis (RA) per year. Despite this influence on public health, epidemiologists continue to struggle to understand OA. Osteoarthritis cannot be systematically prevented or slowed down, and many patients do not improve significantly from symptomatic therapies. A disease-modifying therapy for OA is currently unavailable, and the medications that are available to treat its symptoms are generally unsuccessful.

Joint symptoms, structural pathology (such as with X-ray), or a mix of the two can all be used to define OA. Joint pain and stiffness are the main symptoms. Although all joint components are affected, the alterations in the proximal bone and the loss of articular cartilage are still the most common manifestations. The radiographic features typically used to define OA include joint space narrowing, osteophytosis, subchondral sclerosis, cyst formation, and abnormalities of bone contour. With another approach, confined compression, indentation, tensile, and shear tests can be used to determine the mechanical properties of cartilage. These characteristics are essential for any investigation of tissue stress. However, cartilage failure cannot be predicted solely by the properties of the material neither.

Aim of the study

The present research work took place for almost it's entirety at the Institute of Biomedical and Neural Engineering - IBNE (https://en.ru.is/bne), at Reykjavik University (Iceland). The main focus was to characterize the mechanical performances of innovative Digital Anatomy materials and thus, explore new possibility for study cartilage diseases such as OA. Those materials, available on the J850 Digital Anatomy Printer from Stratasys, use Polyjet technology to produce three-dimensional printed models of anatomical parts. However, the key feature of this technology is the possibility of mimicking the mechanical properties of the native tissues. The materials able to mimic cartilage tissue, do not come with a commercially available preset and thus, to the best of our knowledge, were still to be designed and tested. In order to do so, two parallels computational and physical approaches were carried out.

Starting from 2D patient-specific segmentations of the knee joint, a 3D model was obtained. The same model was both 3D printed and utilized in a Finite Element Analysis. The physical model was tested (along with standard specimens of the materials) mechanically in a prototype setup that takes into account the patient-specific morphology of bones and cartilage tissue. In the FE environment, this setup was reproduced at the best of our possibilities. The results from computational and physical tests were compared and this served as an inverse validation of the testing setup.

As a first insight of innovative 3D printing technologies in the field of personalized healthcare, the whole process also became the standard workflow for the newly established Icelandic Center for Advanced Additive Manufacturing - ICAAM (https://en.ru.is/icaam) at Reykjavik University. Starting from the 2D medical data acquisition to the model validation, the main steps of the workflow are schematized below (figure 1).

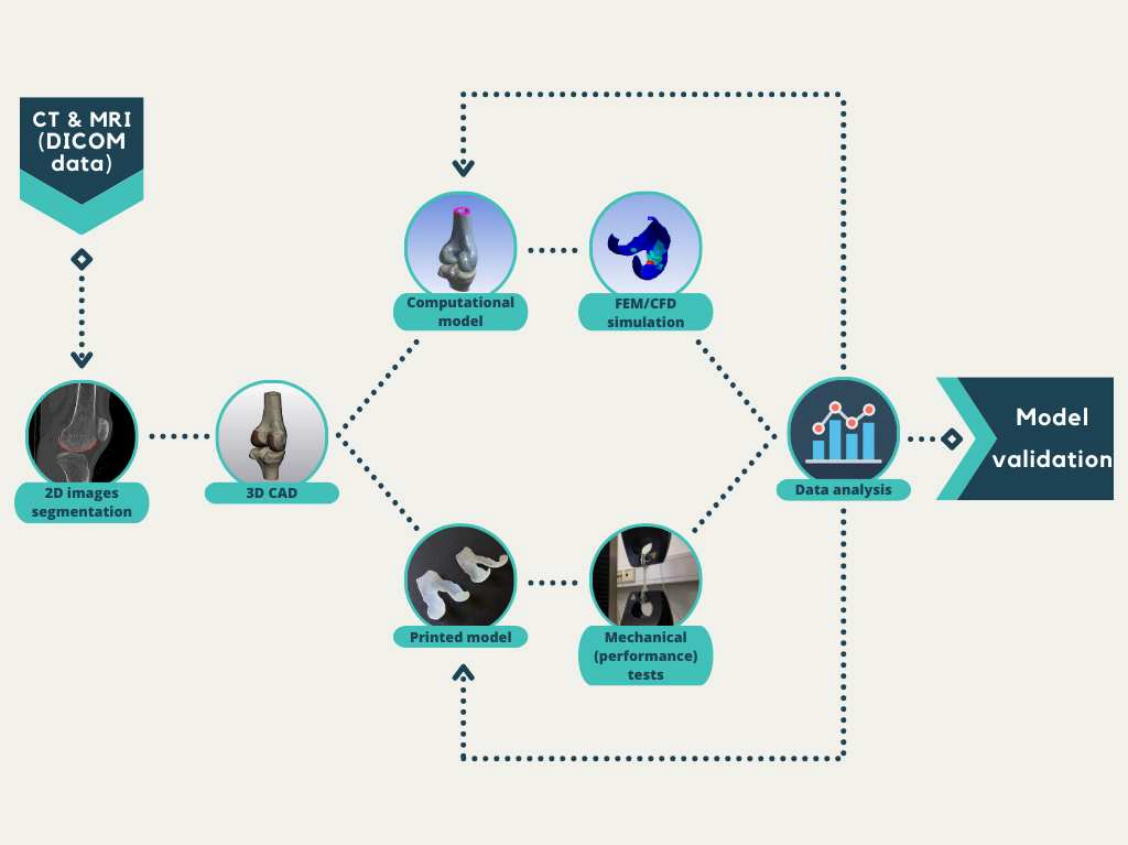

Figure 1: ICAAM workflow.

Thesis composition

The first chapter takes into account theoretical notions and states of art of various fields that were considered important in order to properly understand and contextualize the present research work. Looking at the knee joint from an anatomycal and biomechanical point of view is the first step and it leads to a deeper understanding of the articular cartilage, being it the longest and most important paragraph. Finite Element Analysis, 3D printing and mechanical testing are other crucial tools utilized through the workflow of this research.

More precisely, the second chapter offers a detailed description of the techniques and procedures carried out to produce the results. From the original 2D medical data, to the 3D computational model that was later used in a Finite Element Analysis. Meanwhile, in a parallel approach a 3D physical model was first printed with advanced techniques and then its properties were tested for a mechanical characterization.

The third chapter is about the post-processing of data obtained after this whole process took place, with graphs and tables to offer a detailed overview.

Finally, the results are discussed in the fourth of the present thesis, to understand the validity of the process carried out and how the data obtained can be interpreted.

The work ends with a conclusive chapter to describe the limitations encountered and possible future directions.

Chapter 1

Theoretical Considerations

1.1 Biomechanics and Composition of the Knee Joint

One key part of the musculoskeletal system that helps with the transition and absorption of weight-bearing stresses is the knee joint. This joint is frequently prone to injury or disease, including ligament rupture, meniscal tears, and osteoarthritis, as it is a core component of biomechanical movement. In addition, the knee differs from the other major load-bearing joints in that the main stabilizing factors are soft tissues rather than articular structure. The fact that the joint is divided into three compartments (two tibiofemoral and one patellofemoral) and that menisci are present, which considerably aid in the transfer of contact forces from one articular surface to another, are other noteworthy differences.

1.1.1 Anatomy and Clinical Relevance

The knee joint is a synovial hinge that primarily permits flexion and extension (and a small degree of medial and lateral rotation). It is composed by three bones: patella, femur, and tibia articulating with muscles, ligaments and cartilage structures. Hyaline cartilage lines the joint surfaces, which are contained in a single joint cavity. The tibiofemoral and patellofemoral articulations make up the knee joint. The tibial condyles and the medial and lateral condyles of the femur form the tibiofemoral joint. It is the part of the knee joint that supports weight. The anterior portion of the distal femur articulates with the patella in the patellofemoral joint. It enables the quadriceps femoris (a knee extensor) tendon to be attached directly over the knee, improving the muscle's effectiveness. The patella functions as a fulcrum to boost the power of the knee flexor and as a stabilizing structure to lessen frictional stresses applied to the femoral condyles because it is both formed with and sits within the quadriceps femoris tendon.

In summary, the biomechanics of the knee joint involve a complex interplay between bones, ligaments, muscles, and tendons. The joint allows for flexion and extension, as well as a small amount of rotation and lateral movement, while remaining stable and protected by its ligaments and other supporting structures. But let's see in details the main components of the knee joint.

The bone bridging the hip and knee is known as the femur: it is the largest bone in the human body and is also known as the "thigh bone". It is located in the upper leg, connecting the hip bone to the knee bone, and plays an important role in supporting the body's weight and allowing for movement. The femur is a long, strong bone that has a distinctive shape, with a rounded head that fits into the hip socket and a long shaft that angles slightly outward as it descends toward the knee. At the lower end of the femur, there are two rounded knobs called the medial and lateral condyles, which articulate with the tibia and fibula bones in the lower leg to form the knee

joint. The femur is made up of both cortical and cancellous bone, which provides both strength and flexibility. It is also rich in blood vessels and bone marrow, which produces new blood cells. Injuries to the femur can be very serious and often require medical attention. Fractures of the femur are relatively common and can occur as a result of trauma, such as a fall or car accident. In some cases, surgery may be necessary to repair a fractured femur.

The knee is linked to the ankle by the tibia: also known as the "shin bone", is one of the two long bones located in the lower leg, along with the fibula. It is larger and stronger than the fibula and plays an important role in supporting the weight of the body and allowing for movement. The tibia runs parallel to the fibula, with its upper end articulating with the femur at the knee joint and its lower end forming the ankle joint with the bones of the foot. It is triangular in shape and has several distinct features, including the tibial plateau at the top, which forms the knee joint surface, and the medial malleolus at the bottom, which forms the inner ankle bone. The tibia is made up of both cortical and cancellous bone, which provides both strength and flexibility. It is also rich in blood vessels and bone marrow, which produces new blood cells. Injuries to the tibia can be very serious and often require medical attention. Fractures of the tibia are relatively common and can occur as a result of trauma, such as a fall or sports injury. In some cases, surgery may be necessary to repair a fractured tibia.

Located in front of the knee joint, there's a little bone called the patella: also known as the "kneecap", is a small and triangular bone. It is embedded in the tendon of the quadriceps muscle, and its function is to protect the knee joint and improve the leverage of the quadriceps muscle. At the top of the patella, the quadriceps tendon enters, and the patella tendon exits from the bottom of the patella to insert within the tibia. As the knee bends and straightens, the patella slides up and down over the femur bone, allowing the quadriceps muscle to pull more effectively on the leg. The patella is made up of dense, cortical bone and has a unique shape that allows it to fit perfectly within the quadriceps tendon. It also has a smooth, rounded underside that articulates with the femur bone to form the knee joint. Injuries to the patella can be very painful and can include fractures, dislocations, and chronic pain syndromes. Treatment may involve immobilization, physical therapy, or surgery, depending on the severity of the injury.

The knee's ligaments stabilize the joint, enabling appropriate knee function, since they are strong, fibrous bands of tissue that connect the previous discussed bones together. There are four main ligaments in the knee:

- **Anterior cruciate ligament (ACL)** - located in the center of the knee, helps to stabilize the joint by preventing the tibia (shinbone) from sliding too far forward.

- **Posterior cruciate ligament (PCL)** - also located in the center of the knee and helps to stabilize the joint by preventing the tibia from sliding too far backward.

- **Medial collateral ligament (MCL)** - located on the inside of the knee and helps to stabilize the joint by preventing the knee from bending inward.

- **Lateral collateral ligament (LCL)** - located on the outside of the knee, helps to stabilize the joint by preventing the knee from bending outward.

Knee ligament injuries are common, especially among athletes who participate in sports that involve sudden stops, changes in direction, or jumping. Symptoms of a knee ligament injury can include pain, swelling, instability, and difficulty moving the knee joint. Treatment for a knee ligament injury can vary depending on the severity of the injury, but may include rest, physical therapy, bracing, or surgery in more severe cases.

So, strong fibrous structures like ligaments hold the knee together, and muscles surround it. There are several muscles that are connected to the knee joint and play an important role in its movement and stability. Here are a few of the key muscles that play a role over the knee:

- **Quadriceps muscles**: a muscle group located in the front of the thigh, is responsible for extending the knee. It includes the vastus lateralis, vastus medialis, vastus intermedius, and rectus femoris muscles.

- **Hamstring muscles**: they are located in the back of the thigh and are responsible for flexing the knee. They include the biceps femoris, semimembranosus, and semitendinosus muscles.

- **Gastrocnemius muscle**: located in the calf, crosses the knee joint and helps to stabilize the knee during movement.

- **Popliteus muscle**: is a small muscle located at the back of the knee joint. It helps to unlock the knee joint by rotating the tibia bone slightly during knee flexion.

- **Iliotibial (IT) band**: a thick band of connective tissue that runs along the outside of the thigh and attaches to the lateral condyle of the tibia. It helps to stabilize the knee joint during movement.

These muscles work together to provide stability and movement to the knee joint. They also help to protect the joint from injury and support overall lower limb function.

The knee is a synovial joint, meaning the inside of the joint is lubricated and nourished by synovium, which envelopes the joint. Synovial fluid is secreted by the synovial membrane, which lines the inner surface of the joint capsule. Less than 1 mL of fluid, is typically present in a normal joint. Synovial fluid is a clear, viscous fluid which typically resembles egg white, this similarity is what gives these joints their name, synovia, which means "with egg." The primary function of synovial fluid is to provide lubrication to the joint, reducing friction between the bones and allowing for smooth movement. It also serves to distribute nutrients and oxygen to the cartilage and other tissues in the joint, helping to maintain their health and function. Synovial fluid contains several different components, including:

- **Hyaluronic acid**: This is a large molecule that helps to provide viscosity and lubrication to the joint.

- **Proteoglycans**: These are complex molecules that help to provide cushioning and shock absorption to the joint.

- **Glycoproteins**: These molecules help to maintain the integrity of the joint and provide additional lubrication.

- **Cells**: Synovial fluid contains various types of cells, including white blood cells and mesenchymal stem cells, which help to maintain the health and function of the joint.

Changes in the composition or volume of synovial fluid can occur due to various factors, including injury, inflammation, or degenerative changes in the joint. For example, in osteoarthritis, the quality and quantity of synovial fluid may be reduced, leading to increased friction and wear on the joint. In some cases, joint aspiration, which involves removing synovial fluid from the joint using a needle, may be done to help diagnose and treat joint conditions. Analysis of the synovial

fluid can provide information about the presence of inflammation, infection, or other abnormalities in the joint.

The femur and tibia's smooth ends are covered by articular cartilage, which helps to absorb some of these forces and protect the bones from damage. That is because during movement, the knee joint is subjected to various forces, including compression, shear, and tension. These forces can cause damage to the knee joint if they are excessive or not distributed evenly. For example, arthritis is a result of damage to this surface. Since articular cartilage is one of the main topics of this work, it will be further discussed in a section on its own.

Another unique part of the knee joint located between the femur and tibia is called the meniscus. There are two menisci in each knee, the medial meniscus on the inside of the knee and the lateral meniscus on the outside of the knee. The meniscus serves several important functions in the knee joint, including:

- **Shock absorption**: The meniscus acts as a cushion between the femur and tibia bones, helping to absorb shock and distribute weight across the knee joint.

- **Stability**: The meniscus helps to stabilize the knee joint by improving the fit between the femur and tibia bones.

- **Lubrication**: The meniscus helps to distribute synovial fluid, which lubricates the joint and helps to reduce friction between the bones.

Injuries to the meniscus can occur due to sudden twisting or turning movements of the knee, or due to wear and tear over time. Meniscal tears are a common injury that can cause pain, swelling, and limited range of motion in the knee joint.

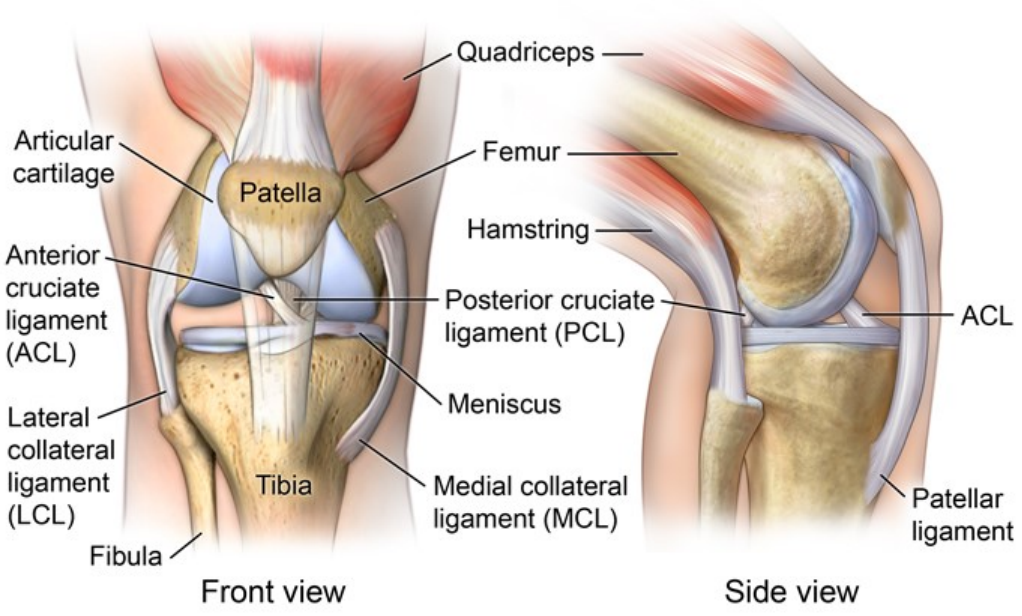

Figure 1.1: Knee joint anatomy detailed view.

1.1.2 Movements and Typicals Load Conditions

The primary motion of the knee joint is flexion and extension, which means bending and straightening of the knee. However, the knee joint also allows for a small amount of rotation and lateral (side-to-side) movement. During flexion and extension, the knee joint undergoes a complex series of movements. As the knee flexes, the femur rotates slightly to accommodate the bending motion.

At the same time, the tibia slides slightly backward, which helps to maintain the stability of the joint. When the knee extends, the femur rotates back to its starting position and the tibia slides forward.

The ACL and PCL play important roles in stabilizing the knee joint during movement. The ACL prevents the tibia from sliding too far forward during extension, while the PCL prevents the tibia from sliding too far backward during flexion. The medial and lateral collateral ligaments, located on either side of the knee, help to prevent excessive side-to-side movement. In addition to the ligaments, several muscles and tendons also help to stabilize the knee joint during movement. The quadriceps muscle, located at the front of the thigh, helps to extend the knee, while the hamstrings, located at the back of the thigh, help to flex the knee. The gastrocnemius and soleus muscles, which make up the calf muscle, also help to stabilize the knee joint.

The forces that the knee joint transmits have significant clinical implications. Obesity is linked to both a higher prevalence of osteoarthritis and a faster rate of disease development because it raises the overall magnitude of stresses across the knee [1],[2],[3],[4],[5],[6]. When walking normally, the knee joint is subjected to forces that are between two and three times body weight. The high moments produced at the knee, the dynamics of acceleration, and the simultaneous contraction of numerous muscles all contribute to this. The net result of each kilogram of added body weight is therefore multiplied by two or three at the knee. Osteoarthritis progression is also linked to lower extremity malalignment, which overloads one compartment at the expense of another [7],[8],[9].Increased peak adduction moments at the knee have been linked to pain, radiographic progression, and indicators of disease severity in motion analysis studies, which measure the external moments of the knee [10],[11]. A 50 % increase in the force transmitted across the medial tibiofemoral compartment can be caused by as little as a 3 to 5° increase in tibial varus alignment, despite the fact that these changes in adduction moment are minor [12]. There has been a lot of interest in the estimation of knee forces.

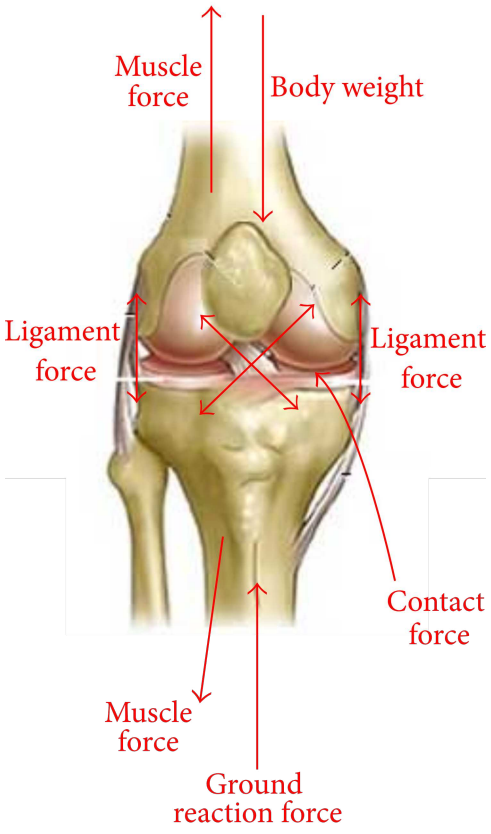

Figure 1.2: Schematization of the forces acting on the knee joint.

Modeling techniques have ranged from two dimensions to three dimensions, with or without soft tissues, with or without simulating contact, and with or without taking into consideration muscle contraction and antagonistic effects. The inverse dynamics method calculates the forces and moments around the joint using experimentally determined motion analysis and external reaction forces [13]. The contribution of muscle forces to the total joint forces is then calculated in order to balance joint moments. The forward dynamics method directly predicts kinematics by using muscle forces and activations, which are subsequently validated by comparison to measured kinematics. Direct measurement of knee forces is an alternative to computational knee force prediction. Measurement in vivo in patients undergoing total knee arthroplasty is now achievable thanks to developments in smart implant technology and telemetry devices. Numerous research have made an effort to calculate forces around the knee during different exercises. Inverse dynamics, forward dynamics, and static body analyses have been found to be the most effective methods for connecting knee kinematics and external forces to internal joint contact forces [14],[15],[16],[17],[18].

The issue of multiple muscles in the same anatomycal district, which makes it challenging to identify specific solutions for knee forces, poses a significant challenge for the majority of musculoskeletal joints in general and the knee in particular. This problem has frequently been solved using EMG-driven and optimization techniques [19],[20]. Wide variations in projections, even for the same activities, have been caused by the diversity of methodologies, solution algorithms, and modeling assumptions. Isokinetic knee extension has been researched as one of the open kinetic chain activities because of how straightforward it is to describe. Peak tibiofemoral compressive forces up to 9 times body weight (BW) were determined by a two-dimensional static study of maximum voluntary isokinetic knee extension with a single quadriceps muscle [17] On the other hand, peak compressive forces of only 4 BW were predicted by a two-dimensional inverse dynamics model utilizing a linear optimization approach to solve for the distribution of synergistic muscle forces [21]. For a number of activities, examples of diverging forecasts could be identified. A static free-body analysis in the sagittal plane projected maximal compressive forces of 5 BW during an open kinetic chain extension exercise and 4.5 BW during a closed kinetic chain extension exercise when comparing open kinetic chain to closed kinetic chain knee extension [22].

However, a three-dimensional inverse dynamics model using motion analysis, force plates, and EMG (quadriceps, hamstrings, and gastrocnemius) predicted higher knee forces during the closed kinetic chain task, peaking at an average of 6.7 and 6.3 BW for the squat and leg press, respectively, as opposed to 5 BW for open chain knee extension [22]. Peak forces for no-resistance squatting were determined at 4.2 BW [23], while forces at maximal flexion for squatting with heels up and down were 2.8 and 3.8 BW, respectively [24].

Despite being a frequent action, walking is difficult to depict. In the initial publication on forecasting forces during walking, which revealed peak forces that averaged 3 BW [14],[15], the challenge was eased by grouping muscles based on comparable function. Peak forces between 1.7 and 2.4 BW have been observed in other research that grouped muscles with similar functions [25]. Peak force predictions nearing 7 BW [26] were obtained by using an objective function to address the redundancy problem that minimized overall forces and moments. During level walking, tibiofemoral contact forces varied between 4 and 6 BW and were sensitive to the amounts being minimized [27].

1.2 Articular Cartilage Tissue

As previously introduced, the bearing surfaces of healthy synovial joints are made of articular cartilage, which spreads the applied load because it has a far better compliance than the bone to which it is attached and permits relative movement of the two opposing bearing surfaces with the least amount of wear and friction. Articular cartilage, also known as hyaline cartilage, fibrocartilage, and elastic cartilage are different types of cartilage based on their chemical makeup. Structures like the ear and the trachea benefit from the elastic cartilage's ability to preserve their shape. In joints, cartilage serves as a surface for bearing or as a binding agent between bones. The intervertebral disc's annulus fibrosus is an illustration of a fibrocartilaginous joint with restricted movement (an amphiarthrosis). Articular cartilage serves as the bearing surface in the freely movable synovial joints (diarthroses), enabling smooth mobility between neighboring bone segments. Examples of synovial joints are the hip, knee, and elbow. A thin layer of articular cartilage protects the ends of opposing bones in a normal synovial joint (Fig. 3). For instance, the cartilage on the medial femoral condyle of the knee averages 2.21 mm in humans and 0.41 mm in rabbits [28]. Normal articular cartilage is white, with a smooth, glossy surface. In healthy, mature animals, cartilage lacks a blood supply and is aneural.

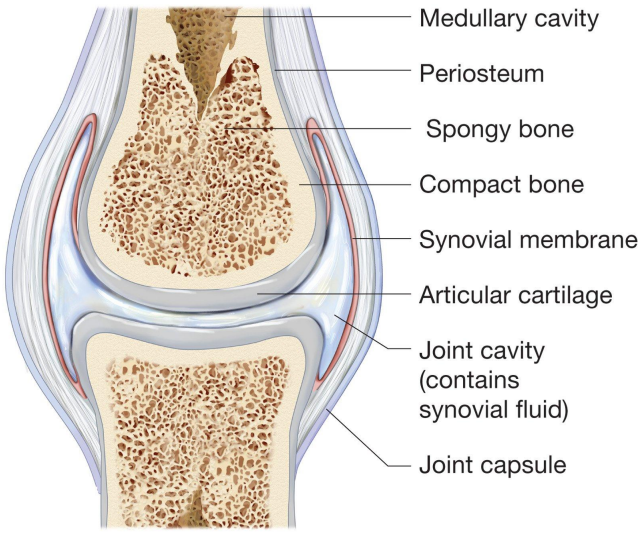

Figure 1.3: Synovial joint schematic representation.

Let's now focus on the biological composition of the tissue: with the smallest cell volume of any tissue in the human body, cartilage has the lowest metabolic activity of any tissue and only comprises about 2% cells. The chondrocytes that make up articular cartilage are a relatively limited number of live cells encased in a complex matrix. Articular cartilage is composed mechanically of a variety of substances with vastly different characteristics. Water makes up between 70 to 85 percent of the weight of the entire tissue. The tissue's remaining components are mostly collagen and proteoglycans. Proteoglycans have a protein core to which chondroitin sulfate and keratan sulfate glycosaminoglycans are joined to create a bottlebrush-like structure. In order to create a macromolecule with a weight of up to 200 million, these proteoglycans can bind to or combine with the hyaluronic acid backbonem [29]. (fig. 4). Proteoglycans make up about 30 percent of the dry weight of articular cartilage. Water content and proteoglycan concentration change with tissue depth. Proteoglycan concentration is comparatively low and tissue water content is maximum close to the articular surface. Whereas the proteoglycan concentration is at its highest and the water content is lowest in the deeper parts of the cartilage, close to subchondral bone [30],[31]. A fibrous protein called collagen accounts for 60 to 70 percent of the dry weight of the tissue. Although

other forms of collagen are found in lesser proportions, type II collagen predominates in articular cartilage [32].

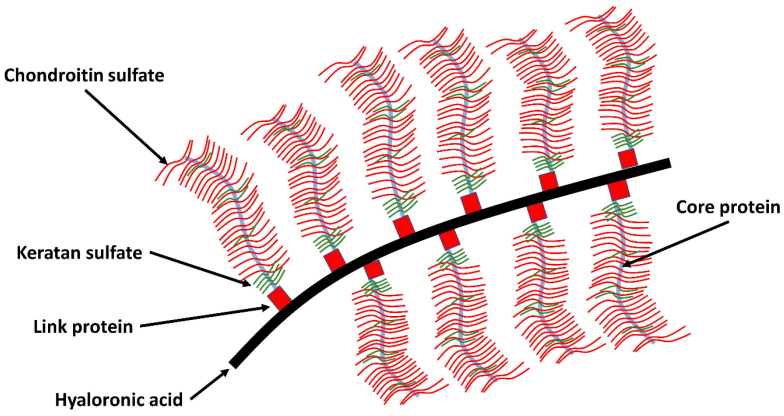

Figure 1.4: Collagen network interacting with the proteoglycan network in articular cartilage.

The depth of the tissue affects the collagen architecture in different ways. Four zones between the articular surface and the subchondral bone are frequently used to characterize the nature of articular cartilage: the surface or superficial tangential zone, the intermediate or middle zone, the deep or radial zone, and the calcified zone (figure 1.5). The line separating the cartilage from the underlying subchondral bone is the calcified cartilage. The tidemark is the point where the deep zone and calcified cartilage meet. The structure of articular cartilage has been shown by optical microscopy, such as polarized light, scanning electron microscopy, and transmission electron microscopy [33],[34],[35],[36]. While each of these approaches shows a roughly comparable collagen orientation for the superficial and deep zones, there is still debate over the collagen fiber orientation in the middle zone.

It is rather evident that cartilage has a mechanical purpose: it offers a bearing surface with less wear and friction, and because of its compliance, it helps to evenly transmit loads among opposing bones in a synovial joint. The contact stresses at a joint would be substantially higher if cartilage were a stiff material like bone because the area of contact would be much less. These mechanical functions by themselves probably wouldn't be enough to support a thorough investigation of cartilage biomechanics. But the apparent connection between mechanical variables in an joint and osteoarthrosis provides great incentive for research into the mechanical behavior of articular cartilage.

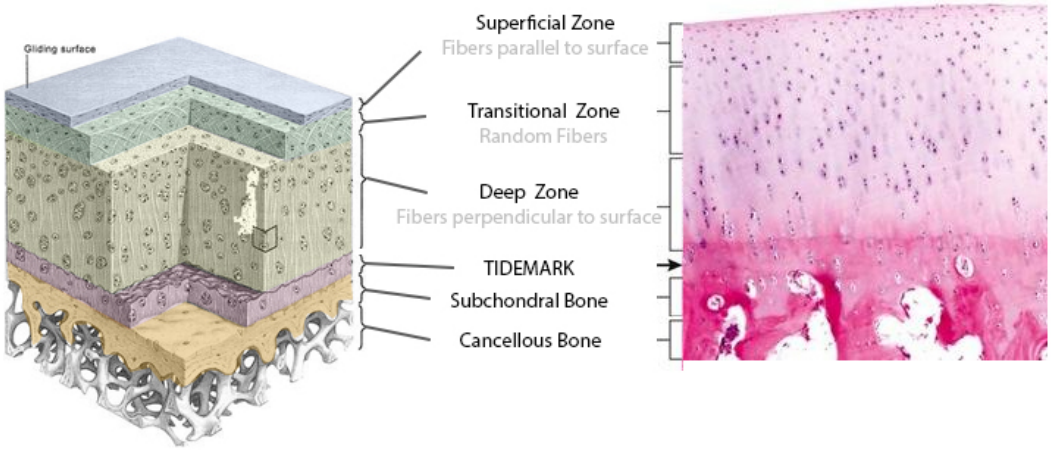

Figure 1.5: Detailed view of cartilage layers variation with depth.

1.2.1 Osteoarthritis

One of the most prevalent musculoskeletal disorders in the older population, OA results in structural tissue deterioration and eventually a loss in function [37]. The most prevalent form of OA, which is the main cause of locomotor disability, affects the knee joint . The condition, known as secondary OA, is influenced by inheritance, aging, gender, obesity, and trauma or damage to the afflicted joint [38] and frequently results in joint replacement [39]. Primary OA is the term used when there is no recognized reason for the disorder [40].

However, depending on the specific criterion utilized and the area of interest, osteoarthritis prevalence varies. The condition mostly affects the knee, hip, and hand joints. As people age, osteoarthritis becomes more prevalent, and beyond the age of 50, women are more likely than men to be affected. Osteoarthritis generally progresses over years, though symptoms may be stable for extended periods during this timespan. Clinical and radiological characteristics are used to make a diagnosis of the illness. The proportion of people without symptoms who have radiological signs of osteoarthritis is about half. Osteoarthritis has long been characterized by a failure of the repair process of injured cartilage as a result of biomechanical and biochemical changes in the joint, in addition to the involvement of many joint tissues. Because cartilage lacks blood vessels, the chondrocytes—the cells in charge of maintaining a substantial amount of extracellular matrix—are only able to receive a limited amount of nutrients and oxygen. Clusters of chondrocytes form in the injured areas at an early stage in an effort to effect a repair, and the concentration of growth factors in the matrix increases. This endeavor ultimately fails, creating an imbalance that is more favorable to degradation. As a result, the tissue begins a vicious cycle in which extracellular matrix creation is outweighed by degradation. Due to the aneural nature of articular cartilage, these alterations do not manifest as clinical symptoms unless innervated tissues are implicated. This is one of the causes of osteoarthritis's delayed diagnosis. Although it has long been believed that cartilage plays a major part in the pathogenesis of osteoarthritis, current research indicates that bone and synovial tissue also play important roles, and patchy chronic synovitis is a hallmark of the condition. Synovial inflammation [41]is hypothesized to be attributable to cartilage debris and catabolic mediators entering the synovial space and correlates with clinical symptoms such joint swelling and inflammatory pain. Catabolic and proinflammatory mediators are produced by synovial macrophages, and inflammation begins to adversely influence the balance of cartilage matrix deterioration and repair. A vicious loop results from this mechanism, which in turn makes synovial inflammation worse. Although it is rarely as severe as in rheumatoid arthritis and occurs in both early and late stages of osteoarthritis, synovial inflammation may contribute to the vicious cycle of progressive joint degeneration.

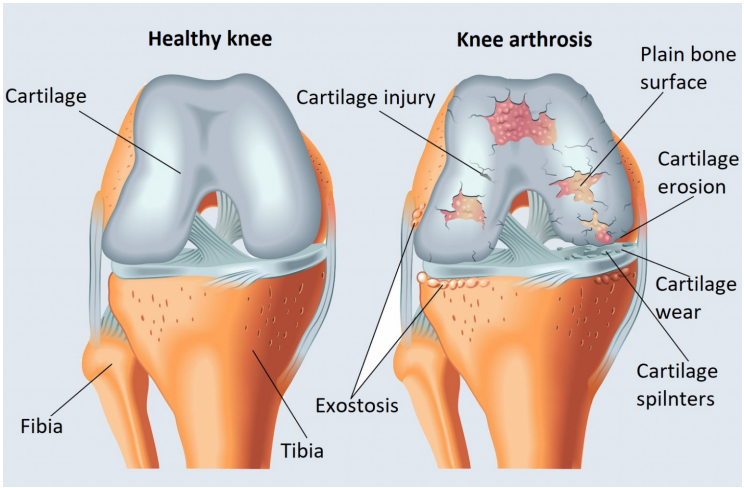

Figure 1.6: Common effects of osteoarthritis on femoral cartilage.

From a clinical and diagnostic point of view, osteoarthritis pain is the primary complaint that drives individuals to their family doctor. Intermittent pain is common, usually worse during and after weight-bearing activities. Throughout the duration of the illness, there may be inflammatory flare-ups. Osteoarthritis patients also experience stiffness, often in the morning, following periods of inactivity, or especially in the evening. Patients also consult their family doctor due to loss of mobility and function. Patients complain of symptoms that make daily tasks including walking, climbing stairs, and doing laundry difficult. Osteoarthritis symptoms may be accompanied by sadness and restless nights, which may increase one's risk of impairment. The patients' quality of life is obviously reduced by osteoarthritis symptoms. To confirm and characterize joint involvement, as well as to rule out pain and functional syndromes with other causes, such as inflammatory arthritis, a physical examination is required. Bony edema, joint effusion, or both can cause joint enlargement. A synovial effusion may be seen throughout the course of osteoarthritis, not just during flare-ups, but also as a recurring symptom. Getting loose objects or cartilage (or meniscus) fragments into the joint space can cause a joint to lock. It is important to be cautious when assigning pain to its proper location; for instance, individuals with hip osteoarthritis may mistakenly report knee pain due to transferred pain or anserine bursitis. Additional spinal and neurological testing is frequently required. Imaging tests are rarely required to confirm the diagnosis, although they may be helpful to determine the extent of joint damage and to track the development of the disease.

Keeping this in mind, it appears still unknown why there is little correlation between clinical traits and structural tissue changes in osteoarthritis. The disparity may be caused by the slow progression of joint tissue deterioration mixed with the insensitivity of current monitoring techniques. In order to better understand the disease and develop therapeutic options, structural alterations assessment is a difficult task. In vivo assessment of early and minimal tissue injury is challenging. Osteoarthritis makes it impossible and frequently contraindicated to perform biopsies on cartilage, bone, and synovial tissue for comprehensive histochemical and biochemical analysis. Additionally, because tissue changes are frequently localized, arbitrary biopsy techniques may overlook them. With the aid of arthroscopic techniques, the cartilage's surface can be observed [42]. Nevertheless, these procedures use intrusive techniques, and it is questionable if it is possible to accurately identify the different stages of cartilage degeneration or regeneration processes. Since plain radiography is quick, simple, and inexpensive, it is the industry standard for imaging osteoarthritic joints. The benefit of radiography is that high-resolution images may be acquired fast and frequently while the patient is bearing weight. Limitations include radiation exposure and the inability to visualize anything other than calcified bone, which only gives an indirect measurement of cartilage thickness and no information regarding synovial tissue.

1.2.2 Mechanical Behaviour and Constitutive Models

Articular cartilage is nonlinear, inhomogeneous, and anisotropic, which makes it different from many technical materials. As a result, it displays a nonproportional constitutive relationship between stress, strain, and time and has varied mechanical properties depending on where it is and how it is pointed. Collagen fibers and proteoglycan gel are the two components that make up the solid phase.

Proteoglycans are polyanionic in an aqueous environment, which means that the molecule has negatively charged sites that result from its sulfate and carboxyl groups. In solution, an aggregated proteoglycan molecule spreads out and takes up a considerable amount of space due to the reciprocal attraction of these negative charges. The tangled collagen framework restricts the volume that proteoglycan aggregates can occupy in the cartilage matrix. In order for cartilage to

respond mechanically, the aggregated molecules must bulge up against the collagen framework. The negatively charged sites on aggrecan are pushed closer together when cartilage is crushed, increasing their mutual repulsive force and increasing the cartilage's compressive stiffness. Since they are more difficult to entrap in the collagen matrix, nonaggregated proteoglycans would not be as effective at resisting compressive stresses. Since the aggregated proteoglycans are less effectively confined, damage to the collagen framework also lessens the tissue's compressive stiffness. The movement of fluid through the tissue has a significant impact on how well cartilage responds mechanically. Fluid travels through the cartilage and across the articular surface when it is distorted [43]. Fluid also flows through the tissue if a pressure difference is introduced across a segment of cartilage [44]. These observations show that cartilage functions like a sponge, albeit one that restricts fluid flow. The modeling of cartilage as a combination of fluid and solid components resulted from the realization that fluid flow and deformation are interconnected [45],[46]. The biphasic model of cartilage describes this.

In this modeling, the solid phase of the mixture is made up of all the solid-like elements of the cartilage, proteoglycans, collagen, cells, and lipids. The fluid phase is made up of the interstitial fluid that is unrestricted in its movement within the matrix. The fluid phase is typically modeled as incompressible and inviscid, meaning that it has no viscosity, while the solid phase is typically modeled as an incompressible elastic material [46]. Due to the quick application of loads, cartilage responds to impacts as a single-phase, incompressible, elastic solid since there isn't enough time for the fluid to move relative to the solid matrix. A viscoelastic model is sometimes used to explain how cartilage reacts to creep, tension relaxation, and oscillatory shear. Even though modeling cartilage mathematically is outside the purview of this chapter, certain examples highlight the basic fluid-solid interaction in cartilage. Early analytical models of articular cartilage deformation were single phase, meaning they did not take into consideration the behavior of time-dependent component. Therefore, it was believed that cartilage was an isotropic and linearly elastic solid [47],[48]. Not all physiological loads are appropriate for this strategy. Single phase models may, however, accurately predict the mechanical reaction of the cartilage layer in two situations: first, during the application of the load when no fluid flows; and second, during equilibrium when all fluid flow has stopped. In an unconfined compression study[49], it was provided a helpful elastic analysis of an articular cartilage layer in a synovial joint that makes it possible to connect stresses, strains, and displacements to the properties of the material, the distribution of loading, and the thickness of the layer. Instead of conducting a biphasic analysis, only the two extremes of the loading history—immediately after a load was applied and when the cartilage had regained equilibrium following loading—were taken into consideration. By structuring the study in this way, it is easier to analyze the consequences of the complicated loading on a synovial joint surface without turning to numerical modeling. When time-dependent effects are taken into account, numerical analysis is necessary even for the relatively simpler experimental geometries. However, more complete models that included the tissue's fluid phase were needed to fully simulate the time-dependent reaction of cartilage: the biphasic models previously mentioned are those. The collagen-proteoglycan matrix, which is a solid phase, and the interstitial fluid, which is a fluid phase, were both described as immiscible phases in the biphasic theory of cartilage [50]. It was supposed that neither phase could compress. It was assumed that the solid matrix would be linearly elastic, permeable, homogeneous, and isotropic. The liquid phase was thought to be non-viscous or inviscid. The linear biphasic model is the name given to this fundamental model. This first formulation was referred to be linear because the permeability coefficient was thought to be constant, regardless of the degree of tissue deformation, even though the material behavior and the solution of biphasic models are not linear. With the addition of a permeability coefficient that was more accurate to physiological behavior and was depending on the tissue's strain, the non-linear biphasic model enhanced this supposition.

One of the essential material characteristics, or biphasic constants, used in biphasic modeling

is permeability, which measures how easily fluid may pass through a media. Poisson's ratio and the aggregate modulus are the two extra variables. The first is a stress–strain relationship that is frequently employed in the investigation of articular cartilage deformation and that can be described in terms of Young's modulus and Poisson's ratio. The behavior of the cartilage tissue as a whole, as opposed to just its individual solid and fluid components which are considered incompressible, is described by Poisson's ratio in this context. Curve-fitting experimental results to master solutions from the linear biphasic theory can be used to evaluate the impacts of each biphasic constant (such as Aggregate Modulus, Permeability and Poisson Ratio of the solid matrix) on the creep behavior of articular cartilage (figure 1.7).

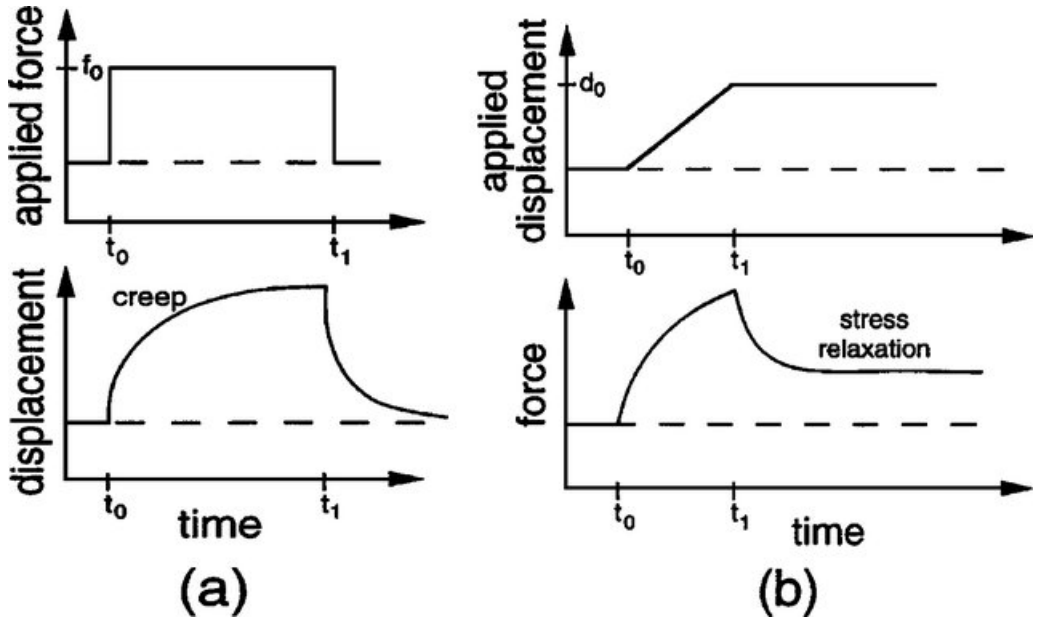

Figure 1.7: Schematics of creep (a) and stress-relaxation (b) viscoelastic behaviors of articular cartilage.

This makes it possible to calculate these constants and demonstrates unequivocally that the permeability dictates the rate of creep and Poisson's ratio defines the curve's "shape" (expressed as a shift factor from the master solution). Infinitesimal strains are an assumption made by both linear and non-linear biphasic models, meaning that the variations in strain are so minor that they can be regarded as linear.

However, physiologically, this supposition is not always true. The majority of physiological loading circumstances (figure 1.8) can lead to significant deformations. To take into account these greater degrees of strain, finite deformation biphasic models have been created. Finite element models have employed these same ideas to characterize the behavior of articular cartilage, much as analytical approaches went from single phase models to the linear biphasic model, the non-linear biphasic model, and the finite deformation biphasic model.

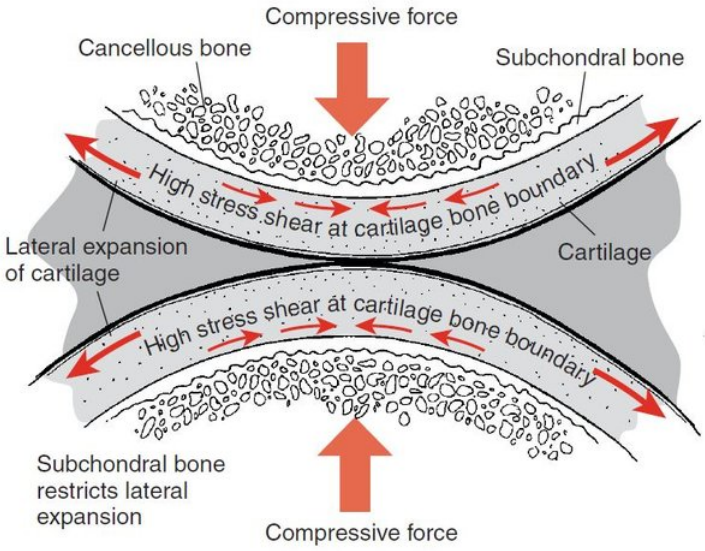

Figure 1.8: Example of physiological loads acting on a synovial joint.

As previously stated, when analyzing the reaction of cartilage immediately following a load application, before fluid has an opportunity to flow, and at equilibrium, when all fluid flow has stopped, cartilage can be modelled as a single phase material (no fluid flow effects). When cartilage may be assumed to be at one of these two extremes of the loading history, it has been modeled as a single phase, linear elastic, isotropic, and homogenous material in various studies. FE examinations of whole articulating joints are one setting in which articular cartilage has been treated as linear elastic. In order to explore stress distributions in cartilage or the surrounding tissues, these have modelled all materials, including articular cartilage, as isotropic and linearly elastic [51],[52],[53]. The hip was modeled [54] to examine the consequences of changes in mechanical properties brought on by osteoarthritis (cartilage softening, subchondral bone stiffening and diminished tribological performance). Variations in the distribution of stress throughout the subchondral bone and cartilage were investigated. It was demonstrated that linear elastic material behavior over extended timeframes, or when physiologically the cartilage would approach equilibrium, was comparable to that anticipated by biphasic models [55].

On the other hand, cartilage can also be expected to act linearly elastically when the strain rate is quite high, as demonstrated in a FE analysis of impulsive loading experiments on rabbit knees [56],[57]. The impact timescale was 20-200 ms as opposed to time-dependent behavior relaxation durations of the order of 1000 s, and the strain rate (0.5 ss') was likewise far higher than that necessary to result in divergence from a biphasic model, therefore once more the choice of a single phase model was justified. The indentation of cartilage was represented [58] as two layers in a cartilage-only FE model: a superficial tangential zone and a mid-zone. To study how osteoarthritis (OA) affects the distribution of stresses, the layers were modelled as linearly elastic, isotropic, and homogenous. The two potential OA side effects that were taken into consideration were localized softening and fibrillation. Fibrillation happens when the cartilage's surface deteriorates to the point that fissures emerge and expand into the deep and middle zones, possibly exposing subchondral bone. From the study was demonstrated that all stresses were often increased as the area just below the indenter softened. This was especially true around the contact radius. One potential explanation for this is because higher deformations would be anticipated to result in greater stress gradients at the indenter edge. Instead of a hemispherical indenter, a planeended cylindrical indenter was used in this investigation. According to another research [59], the primary difference between the two different indenter geometries is that with hemispherical indenters, the contact

area grows with indentation depth, changing the stress distribution. A singularity exists at the contact area's edge but plane-ended cylindrical indenters enforce a continuous contact area, which simplifies the analysis.

As a result, it is challenging to anticipate the stresses in this region accurately numerically, which has ramifications for figuring out how large stress gradients in soft tissue affect failure risk. Additionally, Roth and Mow's research demonstrated that the stress field was unaffected by softening away from the contact zone. Surface stresses decreased due to fibrillation in the area underneath the indenter, while they increased outside of it. Fibrillation therefore appears to lessen the strains brought on by the existence of localized softening. However, the research did not include an explanation of how the FE model reflected fibrillation. It is necessary to use more precise models of cartilage behavior when FE models focus primarily on the time-dependent behavior of the cartilage layer. This is also true when models are contrasted with experimental simulations of cartilage behavior, which frequently use timeframes longer than those of physiological stress.

1.2.3 RESTORE Database

RESTORE's goal is to develop and validate in pre-clinical animal models, solutions for personalised cartilage regeneration and, thus, different strategies are undertaken to overcome the current challenges and unmet clinical necessities in order to design the most efficient solution towards cartilage repair [60]. The RESTORE Project is built upon constructive discussions between orthopaedic surgeons, tissue-engineers, material scientists, cell biologists, small and medium-sized enterprises (SMEs) to co-design an effective approach to manage the specific unmet clinical needs to treat knee chondral lesions. Ten partners from seven countries (Portugal, Spain, Italy, Germany, Sweden, Norway, Iceland and Finland), including Research and Technological Development institutes and two small-medium sized enterprises.

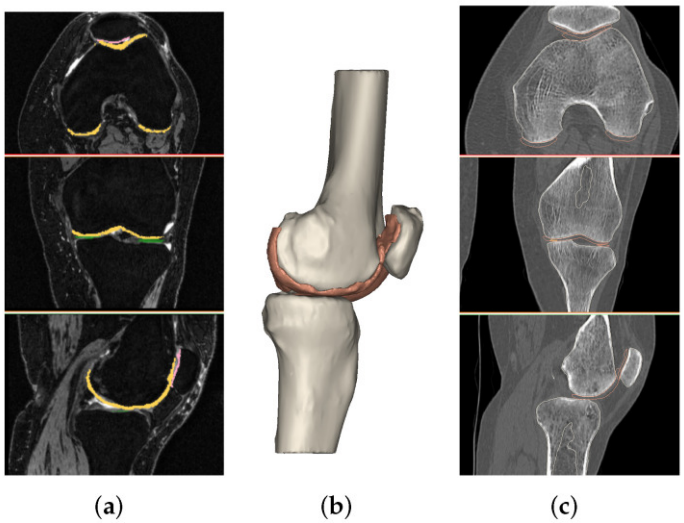

Figure 1.9: Example of data available on RESTORE Database.

The observation of human joint cartilage from x-ray, Computed Tomography (CT) or Magnetic Resonance Imaging (MRI) are the main diagnostic tools to evaluate pathologies or traumas; thus, the database shows a set of novel measurements and 3D features based on MRI and CT data of the knee joint, used to reconstruct bone and cartilages and to assess cartilage condition from a new perspective. The database includes more than one hundred different measurements from 47 individuals (25 females, 22 males). They are divided into three categories: 24 degenerative,

presenting arthrosis or undergoing total knee prosthesis replacement; 15 traumatic, having acute injures; 8 healthy (control group). Using medical imaging software, the bone and cartilage of the knee joint were segmented, and 3D reconstructed (figure 1.9). Several features such as cartilage density, presence of holes was extracted. An exhaustive evaluation made from the 2D images has also been performed. All the extracted features were used with advanced statistics tools and machine learning to test the ability of the model to predict cartilage conditions.

1.3 3D Modeling and Finite Element Method

The finite-element (FE) approach is a numerical stress analysis tool that has been extensively used in both biomechanics and general engineering applications. It functions by breaking down a difficult problem into a series of simpler problems for which there is no analytical solution. This method yields a proximal result since the model can only support a finite number of degrees of freedom. The number of model subdivisions or elements determines how approximate the solution is; a higher number of elements may make it possible to find a more precise solution, but there is a cost in terms of the amount of computational time needed. In practice, a balance between the solution's precision and the available computing resources. Pre-processing, solution and post-processing are the three basic stages of computerized finite element implementations. The user must specify the problem to be solved during the pre-processing stage. The subdivision of the issue domain, or definition of the finite-element mesh, must be provided along with specifics about the geometry, loading, and material properties. In the following stage, which requires minimal user involvement, the computer must solve the specified problem. Post-processing is the third and last phase of any finite-element analysis. Here, the user can alter the data to determine the proper measurements of, for example, stress and strain, and plot chosen values graphically or on contour diagrams. In order to anticipate the loading at which the structure would collapse, this stage may also involve the calculation of design parameters associated to failure. It is no longer typically essential to design specialized solution algorithms for cartilage biomechanical problems due to the wide availability of sophisticated software, but this alternative is always available if necessary.

1.3.1 Application of the finite-element method to articular cartilage

Although extensive research has been done on the biochemistry of this biological tissue, its key mechanical characteristic is that it draws water molecules and swells significantly as a result. This makes it possible to create a tensile stress in the collagen fibers, improving their resistance to the mostly compressive loading brought on by joint movement and preventing buckling-type structural failure. When applied to the study of articular cartilage, FEM can help researchers to better understand the mechanical behavior of this tissue under different loading conditions, such as during walking or running.

To study the behavior of articular cartilage using FEM, researchers first create a computer model of the joint and surrounding tissues, including the bones, cartilage, and ligaments. They then apply loads or stresses to the joint in various directions, and observe how the tissues respond (figure 1.10).

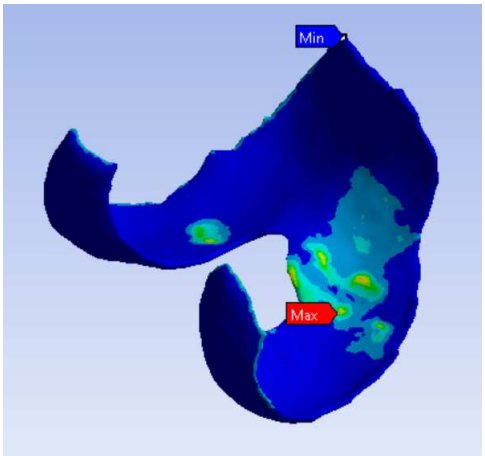

Figure 1.10: Example of stress distribution on articular cartilage in a FEA.

Using FEM, researchers can also investigate how changes to the geometry or properties of the joint or cartilage affect its mechanical behavior. For example, they may simulate the effects of a cartilage defect or injury, or study how joint alignment or loading patterns influence cartilage stress and strain. In order to employ the finite-element technique for cartilage biomechanical assessments, the pre-processing routines require four pieces of data:

1. **The load acting on the joint** such as that produced by movement and muscular forces. The fact that these loads are changing and there is a general lack of information about the dynamic nature of physiological loading presents a special challenge. It's also important to recognize the uncertainties involved in quantifying this input data.

2. **The joint anatomy**: the areas of concern frequently have complicated, three-dimensional geometry. Furthermore, it could differ significantly between people, making it exceedingly challenging to determine, for instance, what value for typical articular cartilage thickness is suitable in a computer model. It will also be necessary to establish the structural relationships and connections between the various load-bearing tissues and structures in the joint.

3. **Material properties**: as was previously discussed, articular cartilage is nonlinear, anisotropic, inhomogeneous, and responds to loading in a time-dependent manner. Therefore, the user must choose representative parameters for the condition being investigated.

4. **Boundary conditions**: what limitations cause the materials and structures in the immediate vicinity placing on the region of interest? The smallest region that would accurately identify the joint anatomy should be modeled because modeling the entire joint surface and underlying subchondral bone could be computationally too expensive in some cases. The model specification will consequently need to take these restrictions from the surrounding material into account.

The best way to comprehend the biomechanical behavior of articular cartilage is to think of it as having two different constituents: a fluid phase and a solid phase. Since the tissue loses fluid when subjected to compressive pressure, the apparent stiffness of the tissue changes over time. Fluid does not have a chance to flow under very brief or instantaneous loading, but some important information can be obtained by modeling the cartilage layer as a linear elastic material using finite elements or analytical methods like Armstrong's perturbation theory approach [61]. Finite-element methods have an advantage in this circumstance because they may be expanded to more intricate geometries and loading configurations that are more representative of the physiological situation. The main focus of single-phase FE models of whole joints has often been on identifying bone stress distributions for bone remodeling predictions. Therefore, despite the fact that a soft-layer model of articular cartilage has frequently been present, it has not received much attention. To summarize, the application of FEM to the study of articular cartilage can provide valuable insights into the mechanical behavior of this tissue under different loading conditions, and help to identify factors that may contribute to injury or degeneration. This knowledge can inform the development of new treatments and interventions for joint-related conditions such as osteoarthritis.

1.3.2 Use of finite elements method in the investigation of osteoarthritis

A frequent type of joint disease and a significant contributor to musculoskeletal pain and disability is osteoarthritis (OA). According to [62], this illness has been defined as follows: Osteoarthritis is the loss of articular cartilage in the parts of the joint that bear most of the weight. It is also characterized by eburnation of the subchondral bone beneath and a proliferative reaction that produces osteophytosis. As a result, OA is initially thought of as an articular cartilage degenerative illness that later results in alterations to the joint's bony structure, particularly with regard to the subchondral bone. These modifications will further affect how the disease develops in the cartilage. It is believed that impact loading of the articular surface is particularly harmful. Instead of hydrostatic stress or volumetric strain, a number of researchers have suggested that the failure criterion be some function of shear stress or strain. This would imply that with isotropic elastic materials, the important local change is not the local change in volume but rather the local change in form of a region. The problem is more complicated in anisotropic materials like articular cartilage, where the hydrostatic and deviatoric components of stress cannot be seen separately. No failure gold standard for articular cartilage has yet been created. However, single-phase models with instantaneous loading have provided some important insights. By increasing local subchrondral stiffness, Brown et al. predicted enhanced stresses in the cartilage layer, and larger shear stresses have also been found near the borders of the joint contact zone.

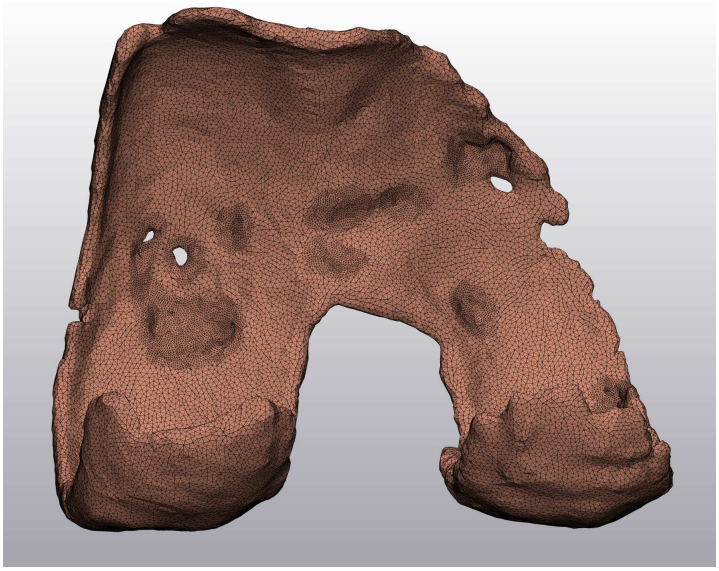

Figure 1.11: 3D model of osteoarthritic articular cartilage that can be used in a Finite Element Analysis.

The stress distribution in loaded articular cartilage is complicated and varies depending on position, location, and direction due to its intrinsic inhomogeneity, anisotropy, and nonlinearity. Therefore, it is difficult to determine the physiological stress distribution because analytical solutions call for a lot of assumptions. Some of these assertions can be disregarded when using the finite-element technique for numerical stress analysis, which offers an advantageous complementary methodology for experimental and clinical studies. Shear stress and strain predictions have given broad indications of the site of failure in experimental osteoarthritis using single-phase finite element models, but specifics of the amount of deformation necessary to begin failure have not yet been clarified.

For example, FEM can be used to investigate how changes in joint alignment, loading patterns, or cartilage properties affect joint mechanics and contribute to the development of osteoarthritis

[63],[64],[65]. Researchers can also simulate the effects of different interventions or treatments, such as joint realignment surgery or the use of joint replacements, to determine their potential benefits for osteoarthritis patients. Furthermore, FEM can also be used to investigate the biomechanics of other tissues while under osteoarthritis condition, such as ligaments, menisci, and subchondral bone [66]. By simulating the behavior of these tissues, researchers can gain a more comprehensive understanding of the factors that contribute to the development and progression of osteoarthritis, and identify potential targets for intervention or treatment.

For example, in [67], a finite element model of the human knee was created in order to assess the impact of osteochondral defect size and location on the stress and strain concentrations around the defect rim. It was consequently possible to determine high-weight-bearing areas and low-weight-bearing areas on the cartilage surface: when compared to osteochondral lesions in LWB areas, lesions in HWB areas resulted in noticeably higher peak strain values. It became clear that severe defects would cause persistent deterioration, making full restoration unlikely. Thus the expected increases in compressive stress in these scenarios showed that there is mechanical overload in the area proximal to the defects.

Overall, the application of FEM to the study of osteoarthritis can provide valuable insights into the mechanical factors that contribute to this disease, and inform the development of new treatments and interventions to improve joint function and quality of life for affected individuals.

1.4 Additive Manufacturing in Healthcare

According to ISO/ASTM standards, "additive manufacturing" (AM), also known as 3D printing, is the process of joining materials to produce parts from 3D model data, frequently layer by layer, as opposed to "formative manufacturing" and "subtractive manufacturing" techniques. A collection of procedures known as three-dimensional printing (3D printing) combine controlled materials to create 3D objects. Usually, this procedure is carried out layer by layer. Another definition of 3D printing describes it as any method for creating 3D things out of layers that are fused together in a row to create a two-dimensional cross-section. With the exception that this occurs in 3D printing by crystallizing, solidifying, or joining a liquid material or powder at any point in the contact of the object that we want to print, the process is very similar to an event during which ink is sprayed on paper in other types of printing as we are familiar with. This approach depends on "computer-aided design," therefore having a computer available to use is also essential for the process (CAD).

The phrase "3D printing" was first used to refer to a particular technology that was developed in 1993 by researchers at the University of Massachusetts, and whose use was subsequently licensed to numerous firms. The first technology to be created was stereolithography (SLA), from which additional techniques like as Powder Bed Fusion (PBF), Fused Deposition Modeling FDM [68], inkjet printing, and contour crafting [69] emerged. The applications for which AM is actively being researched include architecture, medical [70][71][72][73], electronics, automotive, robotics, military and aerospace. Recent advancements in 3D printing have expanded its use in places including laboratories, residences, libraries, and schools. Although there are numerous techniques for 3D printing, these fundamental steps remain the same: making a 3D model of the object to be printed on a computer, using 3D or CAD modeling software is the first stage in the 3D printing process. In some scenarios, reverse engineering and 3D scanning of an existing part can also be utilised.

Making an STL (Standard Triangulation Language) model file is the next step. The model needs to be converted into a format that the printer recognizes, some files must be converted to STL in order to accomplish this. Comparatively speaking to other formats, the OBJ and 3D printing formats are less common. STL format introduces a model to the printer using polygons or triangles. The STL file is loaded into the slicer software, which slices file layers. After getting the model, the slicer transforms it into G-code, which is a set of instructions for CNC machines and 3D printers. The third stage has to do with printing models. There are numerous devices that each print a model piece using a different mechanism. It should be mentioned that in some devices, removing parts is quite easy and problem-free in step four, which is about removing the printed parts. However, this technique is very sophisticated and accurate in more industrialized models. The fifth and last step, post-processing, uses a variety of technologies. For example, a part may need to undergo UV processing in specific circumstances.

Clinicians have employed 3D printing technology to solve a variety of problems related to healthcare and medicine [74]. They can be divided into a number of broad categories, such as the production of specialized surgical instruments, pharmaceutical research on drug fabrication, dosage forms, delivery, production of medical devices, development of customized prosthetics, implants, anatomical models, bio-engineered organs and tissues and surgical planning. The use of 3D printing in medicine offers advantages such as cost-effectiveness, better productivity, and the democratization of design and manufacturing in addition to the ability to customize and personalize medical products, medications, and equipment. One of the most remarkable aspects of this technology in biomedical applications is the personalization of medical products for individuals [40]. An additional benefit of 3D printing in medical applications is the manufacture of intricate implants, prostheses, surgical aids and models. The raw material used in the majority of 3D

printing methods is either made of soft plastic or metal powder. As it is disseminated in incredibly small amounts and fed by a roller or blade installed in the bed where the portion of a model is being created, the powder is often kept in cartridges or beds. The combined thickness of these layers is as thin as the raw material powder particle size, which can range from 1 micron to 5 micron [75].

Early 3D printers could mostly generate very poor sculptures composed of plastic, porcelain, and even plaster. However, as technology evolved, more precise, durable printers could build even metal volumes. At the moment, 3D printers can print polymers, ceramics, and metals using a variety of feedstock types, including as powder, filament, and bioinks. In addition to helping with the fabrication of patient-specific devices, the significant advancements in 3D printing technology have allowed surgeons to address the majority of the problems with the traditional manufacturing methods for medical devices, such as multiple manufacturing steps and expensive tooling [76]. Dentistry, orthopedics, cardiology, pharmaceutics, neurosurgery and tissue engineering are a few of the related fields of applications from the medical point of view.

1.4.1 Digital Anatomy Printers and Polyjet Materials

Digital Anatomy Printers (DAP) are specialized 3D printers that use medical imaging data to create anatomically accurate models of human body parts. These models are created by stacking layers of material on top of each other until the final model is complete. These printers have a high degree of accuracy and detail, making them ideal for surgical planning, medical education, and patient communication. One of the key benefits of digital anatomy printers is their ability to create patient-specific models (figure 1.12). This means that a surgeon can use imaging data from a specific patient to create a model that closely resembles their anatomy. This allows surgeons to practice complex procedures on anatomically accurate models before performing them on the patient, reducing the risk of errors and complications along withe the effective operation time. Digital anatomy printers also have significant benefits in medical education. Medical students can use these printers to create models of human anatomy that are much more realistic and interactive than traditional models. This can help students to develop a better understanding of anatomy and surgical techniques, leading to improved patient outcomes.

Figure 1.12: Example of a heart printed with Stratasys j850 DAP at Reykjavik University.

In combination with DAP, PolyJet is a powerful 3D printing technology that produces smooth and accurate parts, prototypes and tooling. With microscopic layer resolution and accuracy down to 0.014 mm, it can produce thin walls and complex geometries using the widest range of materials available with any technology. PolyJet materials are a type of 3D printing material that uses a combination of liquid photopolymers and UV light to create parts with a high degree of accuracy and detail. It works in a similar way to the printing of inkjet documents, however, instead of depositing droplets of ink onto the paper, the print head deposits layers of a liquid photopolymer on a tray and immediately cures them immediately by means of UV light. The thin layers are overlaid until a prototype or a production part. From the structural point of view, a key benefit of PolyJet materials is their ability to create parts with a high degree of complexity. These materials can be used to create parts with intricate shapes and geometries that would be difficult or impossible to create with traditional manufacturing methods. This makes them ideal for creating anatomical models that closely resemble human anatomy. PolyJet materials also have significant benefits in terms of customization. Because they can create multi-material parts, they can be used to create parts with a range of different properties, such as varying levels of flexibility or transparency, meaning that a single print can incorporate multiple materials with different properties. This allows medical professionals to create models that closely resemble the tissue they are trying to simulate or when parts may need to simulate different types of tissue, leading to better surgical outcomes.

1.4.2 Achievement of Native Tissue Properties

The mechanical properties of native tissues are crucial for their proper function. Digital anatomy printers can mimic these properties by using materials with specific stiffness, elasticity, and tensile strength. For example, printing cartilage tissue requires using materials that are soft and elastic, while printing bone tissue requires using materials that are stiff and strong. Typically, the material characteristics of 3D printed anatomical models have frequently been comparable to human tissue only in shape and not in mechanical responsiveness. With the use of composite printed materials, the new Digital Anatomy Printers technology more accurately imitates the mechanical properties of native tissue.

For what showed in [77], the capacity of the 3D printed myocardium to mimic porcine tissue compliance is promising. Additionally, when tested by puncture, both printed and porcine myocardium failed in a comparable manner. The variability was the main distinction between printed and porcine myocardium. The printed materials are very consistent, as from the results, however the original tissue is rather variable. Every heart has its own set of trabeculae and muscle fibers, which greatly contribute to the tissue's variability. Even though the rigidity of the printed myocardium does not always match that of the tissue, the materials' reproducibility might be a big benefit when employed in bench models for testing. The stiffness value of the myocardium manufactured using DAP exhibits good repeatability both within and between samples. This should make it possible for a bench model made of these materials to perform consistently throughout a test as well as consistently when compared to other similar bench models. Moreover, they exhibit less part-to-part heterogeneity than porcine myocardium: this could enables the materials to be used to build anatomical models to replicate operations for development and training, as well as bench models for device testing.

Simulation of endovascular intervention demands clinical relevancy too, and material jetting 3D printing presents a solution for mimicking vascular distensibility. Within 125 microns, these 3D Polyjet models can reproduce patient-based vascular geometry. As well as being produced in a variety of colors and material stiffnesses, Polyjet 3D printed models can imitate disease states like calcifications or lesions. The vasculature may be printed utilizing a range of compliant materials to

help with the simulation of the biomechanical characteristics of vessel walls. Furthermore, a flow loop with physiologically pressured conditions can be created to use material blasted 3D-printed anatomical models for device testing with a variety of imaging modalities, including planar x-ray, computed tomography, magnetic resonance and ultrasound. In particular, the only method to record the material's non-linear response under pulsatile physiological conditions is through the use of IVUS (IntraVascular UltraSound), which enables the capture of dynamic response. For example, in [78], IVUS analysis of 3D printed vascular models from DAP and Polyjet materials successfully proved the capacity to properly replicate the distensibility of human arteries. The ability to track a device to a desired site, how a stent retains its position within an artery when deployed, or how a device plugs an aneurysm depend critically on the blood vessel's distensibility. Additionally, the usefulness of these models could be further increased by adding controlled mechanical features to vascular anatomical models, enabling meaningful endovascular device testing under predetermined physiological settings.

1.5 Mechanical Characterization

As largely explained in the previous chapter, PolyJet materials are a type of 3D printing material that uses liquid photopolymers and UV light to create highly detailed and complex parts. These materials have a range of applications in the medical field, where they are used to create anatomical models, surgical tools, and other medical devices. To ensure that these materials meet the requirements of their intended applications, it is essential to perform mechanical characterization tests. Mechanical characterization tests involve subjecting the material to various mechanical stresses and measuring its response. These tests can provide valuable information about the material's properties, such as its strength, elasticity, and durability. Mechanical tests can be performed under various conditions, including different temperatures and humidity levels. These factors can have a significant impact on a material's mechanical properties, so it is essential to perform tests under conditions that are representative of the intended application. By performing these tests, engineers and designers can ensure that components and structures are designed to withstand the expected loading conditions over their intended service life.

Some of the most common mechanical characterization tests for industrial materials include:

- **Tensile Testing**: This test involves pulling the material apart in two directions to measure its tensile strength and elongation at break. This test is commonly used to measure the material's stiffness and ductility.

- **Compression Testing**: This test involves applying a compressive force to the material to measure its compressive strength and deformation. This test is commonly used to measure the material's ability to withstand pressure.

- **Flexural Testing**: This test involves bending the material to measure its flexural strength and modulus. This test is commonly used to measure the material's resistance to bending and deformation.

- **Fatigue Testing**: This test involves subjecting the material to repeated cyclic loading to measure its fatigue strength and durability. This test is commonly used to simulate the effects of long-term use on the material.

For most testing types resulting data can be plotted, for example, on a stress-strain curve, which provides valuable information about the material's mechanical properties. The results of these mechanical characterization tests can be used to inform the design of medical devices and ensure that they meet the necessary performance requirements. For example, if a surgical tool needs to withstand a certain amount of force without breaking, the material used to create the tool can be tested to determine its strength and ensure that it meets the required specifications. In conclusion, mechanical characterization tests are essential for evaluating the properties of polymeric materials and ensuring that they meet the requirements of their intended applications. By performing these tests, medical professionals can design safer and more effective medical devices, leading to improved patient outcomes.

1.5.1 Tensile

Tensile tests are a type of mechanical test used to measure a material's strength and mechanical properties under tension. Tensile tests are typically performed on metal, plastic, or composite samples, and are used to determine key properties such as yield strength, ultimate tensile strength,

and elongation at break. The basic principle behind a tensile test is relatively simple. A sample of the material to be tested is mounted into a tensile testing machine and subjected to a uniaxial force along its axis. The applied force is gradually increased until the sample fractures or breaks (figure 1.13, left). When uniaxial tensile force is applied to a solid, the solid stretches in the direction of the applied force (axially), but it also contracts in both dimensions perpendicular to the applied force. If the solid is homogeneous and isotropic, and the material remains elastic under the action of the applied force, the transverse strain bears a constant relationship to the axial strain. This constant, called Poisson's ratio, is defined as the negative ratio of the transverse (negative) to axial strain under uniaxial stress. Poisson's ratio is used for the design of structures in which all dimensional changes resulting from the application of force need to be taken into account and in the application of the generalized theory of elasticity to structural analysis. Tensile properties are known to vary with specimen preparation and with speed and environment of testing. Consequently, where precise comparative results are desired, these factors must be carefully controlled. During a tensile test, several parameters can be measured, including:

- **Yield strength**: The stress at which a material exhibits a specified limiting deviation from the proportionality of stress to strain. Unless otherwise specified, this stress will be the stress at the yield point.

- **Tensile strength**: the maximum tensile stress (nominal) sustained by the specimen during a tension test. When the maximum stress occurs at the yield point, it shall be designated tensile strength at yield. When the maximum stress occurs at break, it shall be designated tensile strength at break.

- **Nominal strain at break**: the strain at the moment of rupture relative to the original grip separation.

- **Modulus of elasticity**: the ratio of stress (nominal) to corresponding strain below the proportional limit of a material. It is expressed in force per unit area, usually megapascals (also known as elastic modulus or Young's modulus). This is a measure of the material's stiffness or resistance to deformation.

At least five specimens for each sample should be tested in the case of isotropic materials. For anisotropic materials, when applicable, test five specimens, normal to, and five parallel with, the principle axis of anisotropy. When testing materials that are suspected of anisotropy, duplicate sets of test specimens shall be prepared, having their long axes respectively parallel with, and normal to, the suspected direction of anisotropy.

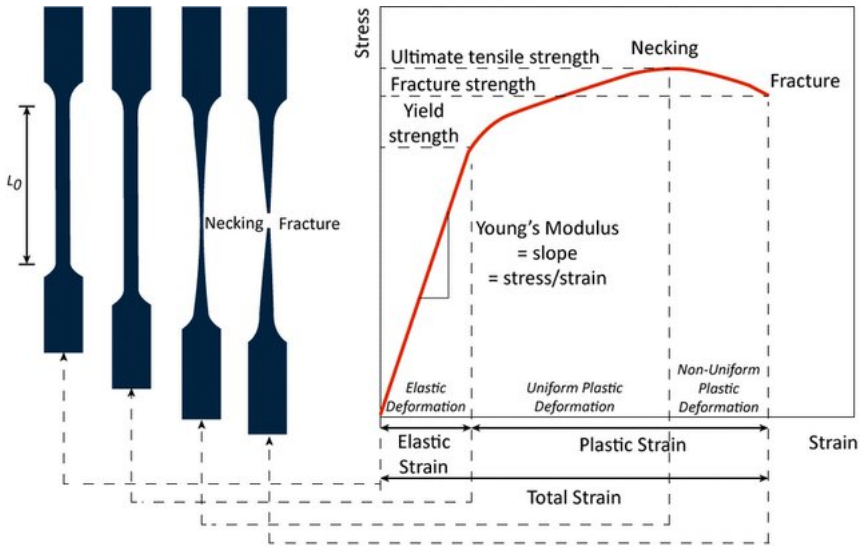

Figure 1.13: Stress-strain curve from a typical tensile test (right) and specimen deformation scheme (left).

This test method is designed to produce tensile property data for the control and specification of materials (figure 1.13, right). These data are also useful for qualitative characterization and for research and development. The results of tensile tests can be used to inform the design of components and structures that are subjected to tension. To put in simple words, if a material has a high ultimate tensile strength, it may be suitable for use in applications where it needs to withstand high stress or loads. Similarly, if a material has a high elongation at break, it may be suitable for use in applications where it needs to be able to undergo significant deformation without breaking.

1.5.2 Compressive

Compression tests are another type of mechanical test, this time used to measure a material's strength and mechanical properties under compression. Compression tests are typically performed on materials such as metals, plastics, and composites, and are used to determine key properties such as compressive strength, yield strength, and compressive modulus. During a compression test, a sample of the material to be tested is mounted into a compression testing machine and subjected to a uniaxial force in the opposite direction along its axis. The applied force is gradually increased until the sample fractures or undergoes significant deformation. Before proceeding with this test method, reference should be made to the ASTM specification for the material being tested. Any test specimen preparation, conditioning, dimensions, and testing parameters covered in the materials specification shall take precedence over those mentioned in this test method. If there is no material specification, then the default conditions apply. The standard test specimen for strength measurements shall be in the form of a right cylinder or prism whose length is twice its principal width or diameter. At least five specimens shall be tested for each sample in the case of isotropic materials. Ten specimens, five normal to and five parallel with the principal axis of anisotropy, shall be tested for each sample in the case of anisotropic materials.

Compression tests provide information about the compressive properties of materials when employed under conditions approximating those under which the tests are made. During a compression test, several and parameters are measured, for example:

- **Compressive strength**: the maximum compressive stress (nominal)
carried by a test specimen during a compression test. It may or may not be

the compressive stress (nominal) carried by the specimen at the moment of rupture.

- **Yield strength**: the stress at the yield point, which is the point at which the material begins to deform permanently.

- **Compressive modulus**: This is the measure of the material's stiffness or resistance to deformation. the ratio of stress (nominal) to the corresponding strain below the proportional limit of a material. It is expressed in force per unit area based on the average initial cross-sectional area.

Materials possessing a low order of ductility may not exhibit a yield point. In the case of a material that fails in compression by a shattering fracture, the compressive strength has a very definite value. In the case of a material that does not fail in compression by a shattering fracture, the compressive strength is an arbitrary one depending upon the degree of distortion that is regarded as indicating complete failure of the material. Many plastic materials will continue to deform in compression until a flat disk is produced, the compressive stress (nominal) rising steadily in the process, without any well-defined fracture occurring. Compressive strength can have no real meaning in such cases.

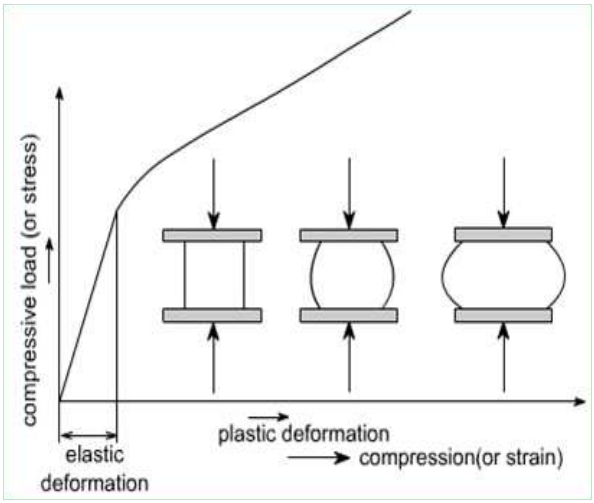

Figure 1.14: Load-deformation curve from a typical compression test.

Compression tests provide a standard method of obtaining data for research and development, quality control, acceptance or rejection under specifications, and special purposes. The tests cannot be considered significant for engineering design in applications differing widely from the load-time scale of the standard test. Such applications require additional tests such as impact, creep, and fatigue. The results of compression tests can be used to inform the design of components and structures that are subjected to compression (figure 1.14). For instance, if a material has a high compressive strength, it may be suitable for use in applications where it needs to withstand high compressive loads. Similarly, if a material has a high compressive modulus, it may be suitable for use in applications where it needs to be able to resist deformation under compression.

Chapter 2

Materials and Methods

2.1 Patient Specific Data

The medical image data were obtained from a previously conducted study [60] and are available on the RESTORE Database (`https://restore-project.ru.is/database`). Participants were recruited as part of the European project RESTORE. The aim of RESTORE is to implement patient-specific solutions for cartilage regeneration. This study has been approved by the Icelandic Bioethics Commission. Now, will follow a description of the procedure adopted during the study in order to extract data from the patients.

At Landspitali University Hospital in Reykjavik, Iceland, 47 subjects (24 females, 23 males, mean age = 50 years, standard deviation = 19 years, minimum age = 20 years, maximum age = 81 years) underwent an X-ray, CT scan, and MRI of one knee using standardized acquisition protocols and patient positioning. 24 patients (12 females and 12 males) ranging from 35 to 81 years, with an average age of 64 years and a standard deviation of 12 years, were diagnosed with degenerative (D) cartilage condition and were waiting to have new prosthetic limbs implanted. In the study, 8 participants (3 females, 5 males, mean age = 34 years, standard deviation = 14 years, minimum age = 24 years, maximum age = 67 years) served as control subjects (C), showing no knee symptoms or history of trauma; while the lasts 15 subjects (9 females, 6 males, mean age = 35 years, standard deviation = 11 years, minimum age = 20 years, maximum age = 50 years) experienced knee trauma (T) with possible cartilage injury. The cartilage from the tibia, the femur, and the patella are processed from the MRI datasets, and the tibial, femoral, and patellar bones are identified from the CT scans. Then, MRI and CT are registered to combine both datasets into a single one.

For the purpose of this work, only control and degenerative subjects were taken into account, with the traumatic ones considered to be less significative in this situation. Among the control [C] and degenerative [D] pools of patients, one subject of each type was selected on the base of the overall quality of the segmentation, thus the quality of the available data, and the representativeness of the pathological (or normal) condition. Gender (male or female) and knee scanned (left or right) were others parameters took into account in order to assure the best comparability of data. Those were the two subjects chosen:

- **PATIENT 18**: condition = D, age = 68, gender = M, knee = left

- **PATIENT 37**: condition = C, age = 26, gender = M, knee = left

From the various anatomical parts, only femoral cartilage, femur and tibia were extracted. The choice was made in order to put the focus on the cartilage itself and to keep the computational and printed models as simple as possible, but this will be further explained in the following chapters.

The 2-Dimensional medical images segmentation was carried out with the use of a professional Mimics Innovation Suite (MIS) software, from Materialise. Materialise Mimics Medical is designed to be used as an image segmentation system and software interface for the transmission of medical imaging data to an output file. Mimics software allows use of 3D visualisation functions that interfaces with all common scanner formats. These models serve as the ideal base for more complex 3D planning, analysis, designing patient specific devices, finite element meshing, and 3D printing. It is indeed possible to import medical picture data (DICOM) and segment the anatomy using the tools to produce precise 3D models (figure 2.1). The software comes with the possibility to select specific bones, to separate them and hide, in order to isolate the direct involved parts that have to be studied in detail.

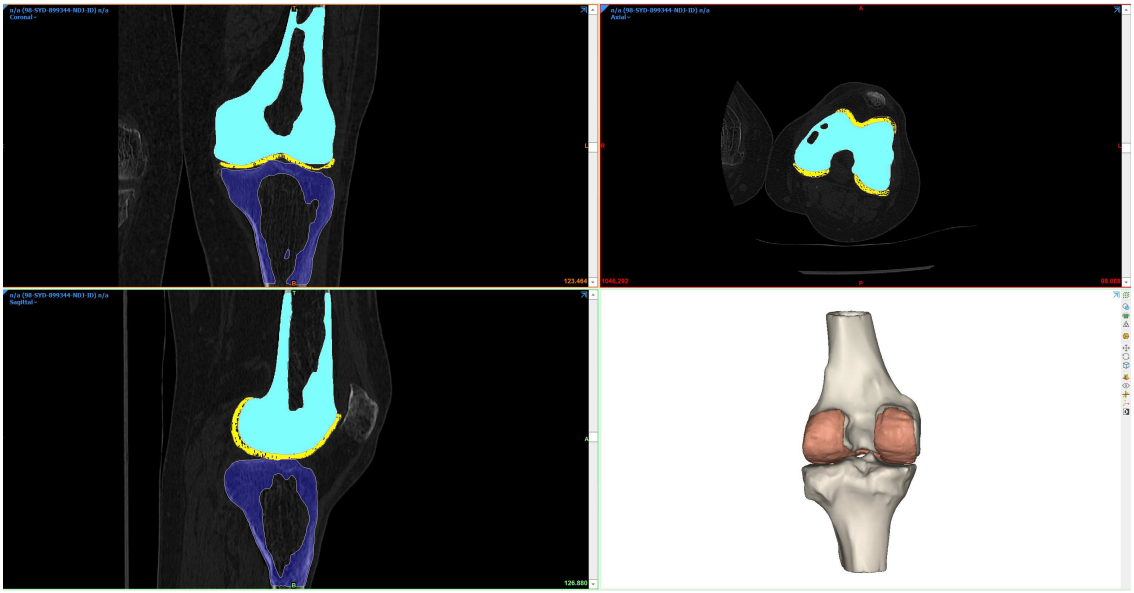

Figure 2.1: 2D planes and 3D preview of subject 18 on Mimics.

Thus, femoral cartilages, femurs and tibias from each patient were isolated and segmented. During the process, some operations like smoothing and mask editing were carried out in order to get the final models more suited for 3D printing and finite element analysis. Once the result was satisfying, output files were produced and directly imported on the Materialise 3-Matic Medical software.

2.2 3D Modeling

Two-dimensional sketches and three-dimensional models can both be produced using CAD software. CAD is used to improve design quality and amount of detail, increase productivity, optimize and streamline the designer's workflow, enhance documentation communications, and commonly contribute to a production design database. 3-matic Medical is designed to be used as computer-aided design and manufacturing software for patient-specific medical, dental, and orthodontic equipment as well as dental restorations.

The software was thus utilized to create surface and volumetric meshes for the studied parts, along with an overall optimization of the geometry in order to properly prepare the model for finite element analysis and additive manufacturing processes. Anatomical supports for mechanical testing were also designed using 3-Matic. After these steps, all the models were converted into .stl and .cdb files for 3D printing and computational analysis, respectively.

2.2.1 Mesh optimization

Geometries of femur, tibia and cartilage were adjusted in 3-matic, enhancing the components' overall quality. Where necessary, local smoothing was done to get rid of unwanted spikes (an artifact of segmentation process). A first reduction in the amount of triangles was made since the 3D surface meshed models produced by Mimics included a lot of triangles with high aspect ratios. At this phase, the *Adaptive remesh* tool was used to create triangular surface meshes on the top layer of bones and cartilage. This tool enables remeshing while maintaining the geometry of an entity. It provides finer control over the generated mesh than *Uniform Remesh* and can even limit the remeshing to a specific area of interest.

Since the analysis is primarily concerned with cartilage, the bones were coarsely meshed to reduce computational costs, while the femoral cartilage was meshed more finely. For the most part, the bone surface was covered with a 2D triangle mesh with a size of 4 mm, while the cartilage was covered with a 2 mm triangular mesh. The bone mesh was eventually developed to a thickness of 2 mm in order to obtain a better load distribution at the intersection area between cartilage and bone end, thus the chondral zone. Moreover, a 1 mm mesh was employed to finely mesh the cartilage regions containing geometric singularities (holes caused by chondral defects, as can be observed in figure 2.2). To guarantee that there were no intersecting bodies present in the models, a Boolean operation of subtraction was carried out. The *Create volume mesh* tool was then used to turn surface meshes into volume meshes to create 3D solid models.

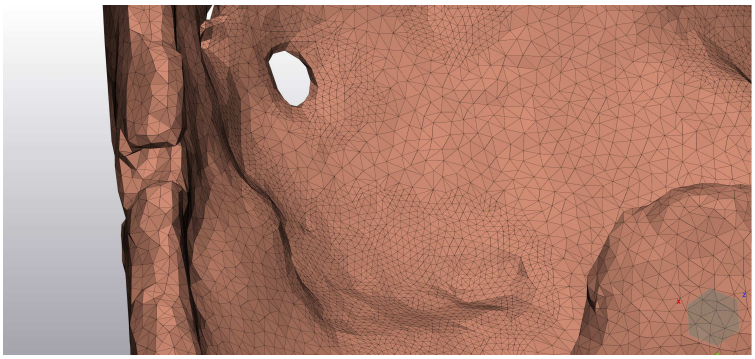

Figure 2.2: Cartilage defects related to tissue degeneration, presenting a finer mesh.

Due to their simplicity and computational efficiency, linear tetrahedral elements (TET4) are frequently employed in FEA. However, because they may exaggerate stiffness and need numerous elements to achieve analysis convergence, if used for cartilage models they may lead to limitations in terms of accuracy. This is due to the fact that TET4 components can only accurately depict a constant strain state and lock for materials that are almost incompressible and bending deformations. Changing the scenario requires the use of higher-order elements. In general, high-order elements (TET10, HEX20) are suggested to create smoother strain and stress estimations in order to better track deformations and stresses in soft tissues like cartilage, muscles, or ligaments. Quadratic tetrahedral elements (TET10) provide a good substitute for simulating articular cartilage in this frame. They provide correct depiction of curved boundaries as their edges and faces can deform while preserving the benefits of tetrahedral mesh production, such as computational efficiency.

Since the bone components of the femur and tibia were of least relevance for our purpose, linear tetrahedral elements (TET4) were employed to produce the volume mesh, instead of quadratic tetrahedral elements (TET10) as for the cartilage. TET4 is the simplest tetrahedron-shaped element with 4 nodes and just 3 translational degrees of freedom (rotations of nodes are ignored). Again, the TET10 element is appropriate for modeling irregular meshes and exhibits a quadratic displacement behavior. In the nodal x, y, and z directions, each node has three degrees of freedom for translation.

Aspect ratio, which is the ratio of an element's longest and shortest sides, and Jacobian, which measures how far an element deviates from its ideal shape, are two characteristics that were computed to assess the quality of the meshes that were produced. This parameters' evaluation revealed that the produced meshes were of an acceptable standard of quality.

2.2.2 Support prototyping

It was decided to prototype the mechanical testing by inserting the distal femur and the proximal tibia in addition to the femoral cartilage in order to accurately simulate the loads that the femoral cartilage endures in real-life circumstances. In particular, anatomically accurate patient-specific supports that could be connected to the testing device were designed and manufactured (figure 2.3). In order to understand which testing setup would have been better between tensile and compressive, we developed two different types of supports. In both instances, we wanted to maintain the testing procedure's integrity, therefore we didn't change the plates for compression testing or the pneumatic grips for tensile testing. Instead, we would only connected the patient-specific supports between the grips or platens and the printed cartilage. The geometry and distribution of the loads present in the patient's knee joint could both be maintained as a result. We came to the conclusion that the supports created for the tensile test were the ideal fit for our assessment after doing many tests directly on the machines. This one, in fact, stayed held in place without the chance of misalignment or wrong positioning both throughout the testing process and after being properly linked to the grips. Reproducibility of a mechanical test must always be ensured, which necessitates minimizing operator-dependent errors. In order to ensure a snug fit for the inserted part, the chosen supports were in fact created to be dimensionally compatible with the size of the grips.

Using the *Create Datum Plane* tool, a cutting plane was made on both the femur and tibia of each patient starting from their segmented 3D models. Then, the datum planes were placed so that the proximal tibia and distal femur were both the same length. The planes were positioned accurately by being perpendicular to the axes that go through the femur and tibia and pointing in the same direction. Then, using the *Cut* tool and the two datum planes as cutting entities, the femur and tibia were cut. Afterwards, two sketches were made using the two datum planes. Specifically, a square and a rectangle were drawn and extruded. Several measurements were taken

before deciding on the proportions in order to properly align the components and adjust the supports to the jaws. The 80 × 80 mm square in particular was created with the intent of providing a surface area sizable enough to guarantee adequate compression force distribution. The 25 x 10 mm rectangle, on the other hand, was created to enable accurate closure between the testing machine's grips and suitable positioning of the square support on the end of the grips. We verified that the distances between the vertices of the two extruded squares were equal in order to ensure that the produced supports were aligned correctly in space.

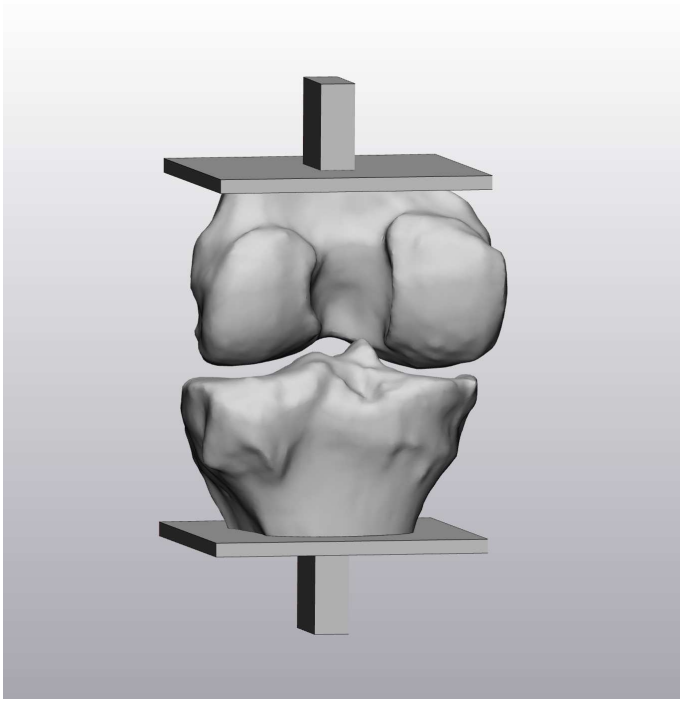

Figure 2.3: 3D view of supports design based on patient 18 anatomy.

2.3 Finite Element Analysis

From the Materialise 3-Matic software, models of femur (support), tibia (support), and femoral cartilage were exported as .cdb file format and imported into ANSYS software. Here, the different parts were assembled into a single model and material properties, loads and boundary conditions were assigned. The tibial cartilages, menisci, and ligaments were left out of the research because this study focused solely on the reaction of the femoral cartilage to specific loading circumstances. Although these components are crucial to the general function and health of the knee joint, their absence allowed for a more straightforward and computationally efficient formulation. In a complementary approach that is discussed in another work (Dr. Damiano Coato's Master Thesis) this computational replication of the testing setup was compared to a model having native morphology (and thus, no supports) and material properties from literature.

Ansys Mechanical enables to solve complex structural engineering problems, it allows for a parameterization of finite element analysis (FEA) solvers to assess various design scenarios and personalize and automate solutions for structural mechanics challenges. From setting up geometry for analysis to attaching extra physics for even higher authenticity, Ansys Mechanical delivers a dynamic environment with a full variety of analysis tools.

2.3.1 Material properties

In order to determine the material's characteristics, experimental techniques were used in conjunction with a literature review. Mechanical testing was conducted to establish the two digitally designed materials' tensile and compression properties after printing standardized samples. Following processing, the data was used to determine each material's Young's modulus (for compression) and Poisson's ratio. The cartilage utilized in the finite element analysis were given these extracted properties. By analyzing the equivalent setup used for prototype tests, with test-derived properties assigned to the cartilage and anatomical supports, the performance of the model was compared and validated. For each material, a *Linear Elastic* > *Isotropic Elasticity* constitutive behaviour was selected and Young's Modulus and Poisson's Ratio were specified as mechanical parameters.

Cartilage tissue

The mechanical response of cartilage to dynamic loading can be modeled as an elastic isotropic material. This is because cartilage's viscoelastic time constant, which is 1500s, is significantly longer than the loading period of interest, which corresponds to the moment at which a fully extended leg touches the ground. The cartilage was simulated with a linear elastic isotropic behavior for this assumption and similar researches from the literature, with a Young's modulus and a Poisson's ratio calculated from mechanical tests.

Bone tissue

In many FEA experiments that are accessible in the literature, the influence of bones properties on cartilage behavior was negligible since their stiffness and density are significantly higher than those of soft tissues. For this reason, despite its well-known heterogeneous and biphasic composition, bone is frequently represented as a linear isotropic elastic material in order to optimize the analysis. Moreover, the distinction between cortical and trabecular bone is negligible when the focus is solely on cartilage. The femur and tibia were both modeled with a linear isotropic elastic behavior with Young's modulus and Poisson's ratio calculated from mechanical tests, for the aforementioned reasons.

2.3.2 Contact definition

When simulating the interactions between various parts of a structure or system in a FEA, the *Contact* and *Target* surfaces selection is a crucial factor to take into account. Generally speaking, the Target surface is intended to remain fixed, but the Contact surface is supposed to move or deform when loaded.

In ANSYS, five types of contact definitions are available: Bonded, No Separation, Frictionless, Frictional and Rough. The term "Bonded" refers to a connection between the two bodies such that their surfaces are tightly joined and they are unable to slide or detach from one another. In the native biological environment, cartilage tissue is attached to the terminal part of the bones in the subchondral zone. In this zone, a transition from the mineralized structure of the bone to the collagenous-made structure of the cartilage occurs. Moreover, the knee is securely kept in place by muscles and ligaments that make sure all surfaces are in close touch with one another, almost as if they were glued together. In short terms, the analysis is made easier, the computational complexity is decreased, and applying loads and boundary conditions is made simpler by defining this contact as Bonded. Significant movements or sliding are not observed, despite the possibility of modest motions and sliding between the two surfaces. This assumption can therefore be expanded to include the contact between the tibia and femoral cartilage as Bonded.

As was previously indicated, because the tibial cartilages and menisci were not taken into account in the analysis, there was a geometrical gap in the contact between the femoral cartilage and the tibia. A *Pinball Radius* was then assigned based on exact (digital) measurements of the separation between the two bodies, bridging the gap as a result. For instance, the degeneration model's Pinball Radius was set to 1.7 mm whereas the control model's Pinball Radius was defined as 1.5 mm. By analyzing only the nodes inside the pinball region and not all the nodes on the body, the Pinball Radius improves the speed of the contact analysis.

As a calculation method for the contact behaviour, the *Augmented Lagrange* formulation was used for the contacts between femoral cartilage and bony supports.

2.3.3 Loads and boundary conditions

In order to analyze the knee joint in full extension, flexion-extension (in the sagittal plane) and varus-valgus (in the coronal plane) rotations for the femur were limited. To accomplish this, a *Remote Displacement* was applied on the femur to limit the rotations along the x, y, and z axis, as well as the translation along the x and y axis. This left only one unrestricted translation along the z-axis. With a *Fixed Support*, the tibia support was constrained at the lower surface (figure 2.4). The top surface of the femur support was subjected to a compressive force of 1150 N along the longitudinal direction (figure 2.5), which corresponds to the force acting during the gait cycle at the position of full extension.

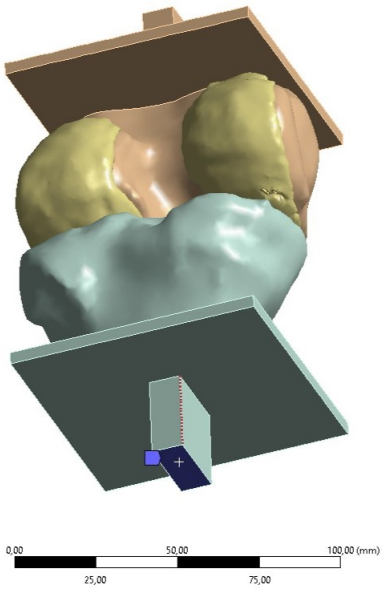

Figure 2.4: In blue, fixed support applied on the lower surface of the tibia.

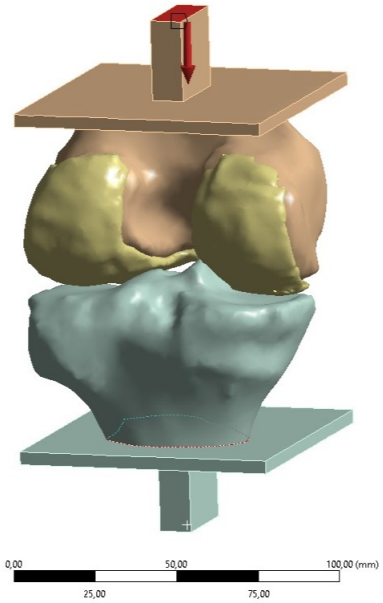

Figure 2.5: In red, compressive force applied on the upper surface of the femur.

2.4 Advanced Additive Manufacturing

2.4.1 3D printers

Stratasys J850™ Digital Anatomy™ 3D Printer

With a printing volume of 490 x 390 x 200 mm, this 3D printer makes it possible to obtain a very coherent and accurate representation of the targeted pathology. It offers, for example, the possibility of reproducing cardiac structures, blood vessels, muscoloskeletal areas, but also of simulating the response of real organ tissues. All these possibilities allow users to realize several applications. For example, it is possible to observe the precise biomechanical behavior associated with age, gender, ethnicity and other pathological and physiological characteristics or to precisely examine bone joints with variations in spongy and cortical density. Compatible with a wide range of thermoplastics, both soft and stiff, the Digital Anatomy range of materials enables the 3D printing of fully customized medical models to achieve realistic anatomy to the eye and to the touch.

Figure 2.6: J850 Digital Anatomy Printer design.

The printer (figure 2.6) operates as follows: the printing block moves along the X-Y axis in order to maximize the printing area coverage and reach the entire build platform. The Build Platform moves in z direction layer by layer in order to build the entire geometry. Drops of liquid Photopolymer are deposited on the building tray by the Printing Block, layer by layer. Exposure to UV light, initiates a very fast polymerization reaction turning the liquid photopolymer into a fully cured ready to use 3D model.

Figure 2.7: Detailed view of a degenerative cartilage printed with the J850.

The J850 DAP was used to print the cartilage models from degenerative and control subjects. 10 model were printed for each subject, 5 with the soft material (expected to mimic the degenerative behaviour) and 5 with the medium material (expected to mimic the healthy behaviour), for a total of 20 printed cartilage models (figure 2.7). For the mechanical characterization, 5 standardized samples for D695 compression test for each material were printed, for a total of 10 samples. 10 standardized samples for ASTM D638 were printed for the tensile testing, 5 for the soft material and 5 for the medium stiff material.

Stratasys Objet260 Connex3™

The Objet260 Connex3 3D printer (figure 2.8) uses Polyjet technology to print models simultaneously with different materials. Printing models with combinations of basic materials (digital materials) allows you to choose from a wide range of available mechanical properties, from flexible to rigid, as well as colors. You can even print models made from different materials on the same build tray in the same print job, and quickly switch between print jobs using loaded model materials. The Stratasys Objet260 Connex 3 has a build volume of 255 x 252 x 200mm and it was used to print the anatomy-shaped supports for the mechanical tests with VeroWhite material. As stated in the past chapters, the supports were designed on 3-Matic for a total of 4 supports, a femur and a tibia for each subject and thus for each morfology studied.

Figure 2.8: Objet 260 Connex 3 design.

2.4.2 Printing software

GrabCAD Print is the most comprehensive available software solution for Stratasys 3D printers. It is a straightforward and intuitive software which makes it easier to prepare, schedule, monitor, and report on print jobs. GrabCAD Print delivers a productive workflow that simplifies job administrations using Stratasys FDM and Polyjet printer since it can read and comprehend CAD files natively. GrabCAD Print reads native CAD and STL files including those created from segmented DICOM data sets and modeling software. The software has an unique voxel based engine that eliminates the need to re-design micro-structures for each new pathology, offering predictable performances with each anatomy choice.

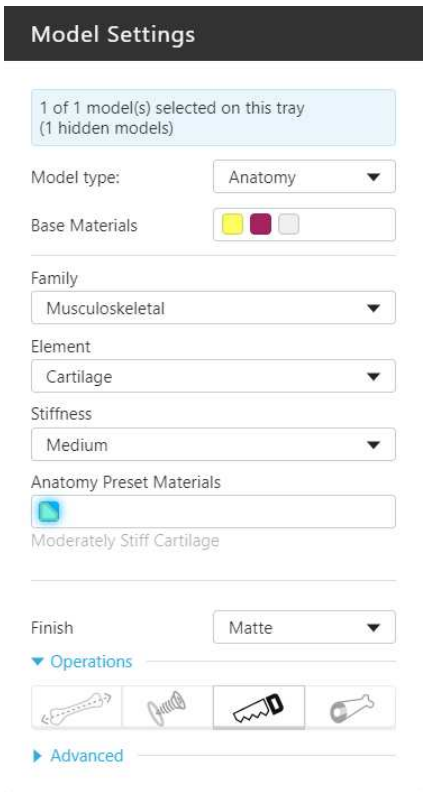

Figure 2.9: Model settings window on GrabCAD software.

For medical purpose, GrabCAD Print offers the most complete library of human anatomy presets, reducing the need to design internal structures. The preset anatomy menu offers more than 100 options that allow you to print accurate, lifelike models by simply choosing the desired anatomy. It also allows the user to add custom designed materials as showed in (figure 2.9). You can choose specific digital anatomies such as, for example, bones, blood vessels and hearts. Some others notable features are the followings:

- the possibility to monitor detailed views of your model and tray, togheter with a slice preview in order to can make necessary adjustments before printing.

- a unique voxel based engine that eliminates the need to re-design micro- structures for each new pathology.

- geometry-targeted tools to create purpose-built parts that minimize weight and material without compromising strength.

- organize print schedule based on estimated job duration, part priority, material consumption and other key considerations.

For our purpose, several models were arranged on the tray as can be seen in (figure 2.10) and printed simultaneously for a more efficient print job in terms of time and material consumption. The digital material selected were *soft cartilage* and *moderately stiff cartilage* (called *medium* in this work for the sake of simplicity). Those materials were designed and provided by a Stratasys engineer as .adm file format and uploaded on the software through the Digital Anatomy Creator tool. Every piece, from the cartilages to the standardized samples, were printed with a matte finish. This is useful for applications where a uniform surface finish is desired. On the other hand, the glossy finish is more suited when very delicate features that cannot be easily cleaned are present. Although the cartilages were very thin in some points, it hasn't been considered to be an obstacle during the cleaning process and thus the glossy finish wasn't needed in this case.

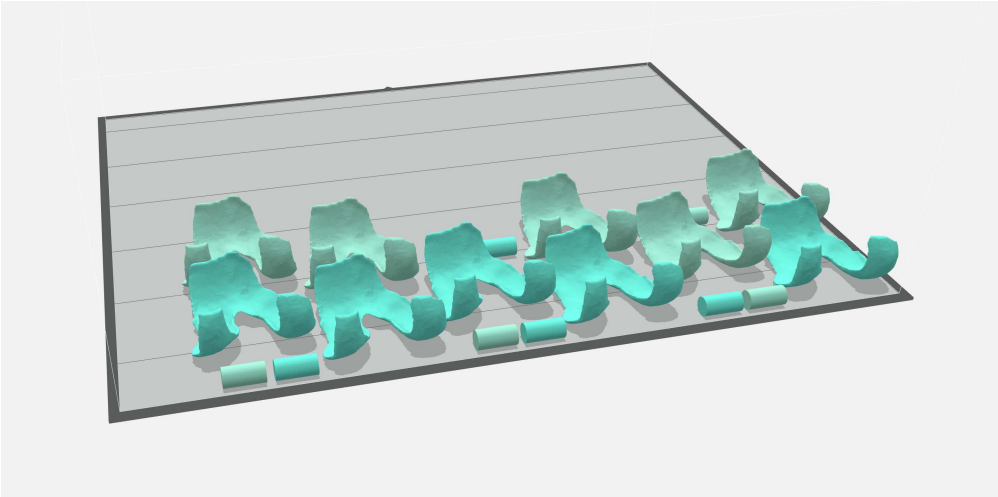

Figure 2.10: GrabCAD tray filled with control cartilages and D695 samples.

Objet Studio is another application for preparing print jobs on Stratasys 3D printing systems, specifically suited in our case for the Objet260 Connex3. The interface is divided into two main screens: On the Studio screen, source files are prepared for production on the printer. The Manager screen displays the queue and status of all jobs sent to the 3D printer. Compared to GrabCAD print, this is an older software and doesn't allow for the design of digital anatomy materials. This is the reason why it has been used to handle the printing queue for the anatomical supports printed with Objet260 Connex3 (figure 2.11). Each support was printed with the *single material — VeroWhite* option and with a matte finish, prioritizing the uniformity of the printed surface.

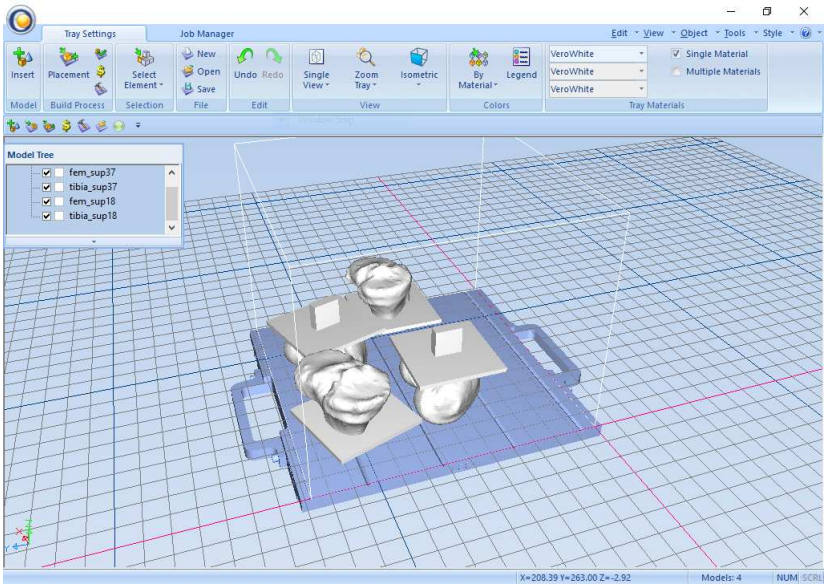

Figure 2.11: Objet Studio tray prepared for the anatomical supports print job.

2.4.3 Printing materials

PolyJet technology is based on Photopolymer resins, UV light and motion working simultaneously in order to produce precise full color and functional 3D models (figure 2.12). The Digital Anatomy material family includes a collection of materials that can be used to mimic human tissue. These materials can be mixed in various ratios with others PolyJet materials like the Vero family and

Agilus30 to provide a variety of shore values that can be used to create virtually any human body anatomy. This class of materials opens up new opportunities to enhance medical modeling, including the ability to educate, suture, puncture, drill, stretch, and conduct mechanical tests for research and medical practice on models with mechanical properties comparable to any type of tissue.

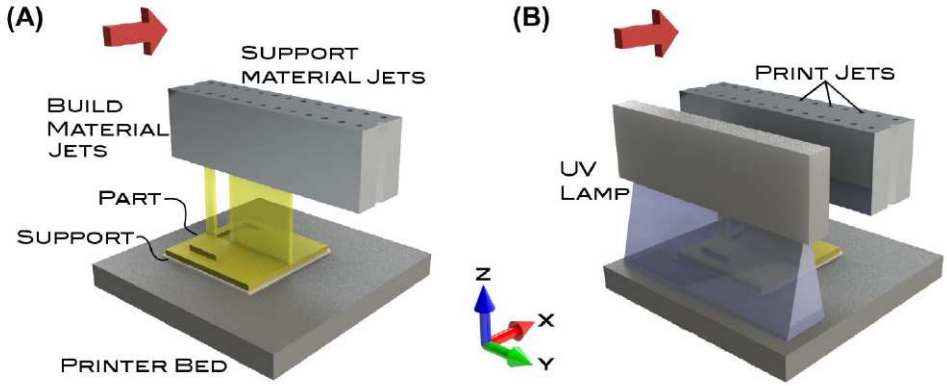

Figure 2.12: Polyjet printing technology schematized.

The mixes of materials used to replicate the characteristics of native cartilage tissue were provided by Stratasys. Those materials, "Soft Cartilage" and "Moderately Stiff Cartilage" (= "Medium"), were designed to emulate the mechanical response of osteoarthritic and healthy cartilage, respectively. The composition is made by different percentages of the Digital Anatomy BoneMatrix and GelMatrix materials, along with PolyJet Agilus30 material (figure 2.13 and figure 2.14)

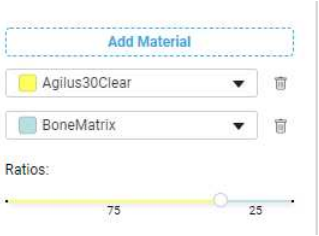

Figure 2.13: Composition of the *Moderately Stiff Cartilage* material.

Figure 2.14: Composition of the *Soft Cartilage* material.

BoneMatrix™

It is a tough, flexible material with memory to maintain its shape. Musculoskeletal models are intended to match bone density characteristics and behave like native bone when force is applied such as discectomy, drilling, reaming or sawing. BoneMatrix creates complex material depositing patterns that mimic porous bone structures, fibrotic tissues, and ligaments.

Properties	BoneMatrix
Printer	Digital Anatomy™ Printer
Print Mode	High Mix, High Speed
Support Material	SUP706
Number of UV Lamps	2
Color	Translucent
Impact, J/m	58.0±4.5
HDT, °C	40.9±0.7
Curling, mm	0.8
Tensile Strength, MPa	28.7±1.6
Strain at Break, %	60.0±6.9
Tensile Modulus, MPa	1059±31
Flex Strength, MPa	29.4±0.9
Flex Modulus, MPa	1102±104
WA, %	4.5

Figure 2.15: Technical information about BoneMatrix material.

Agilus30Clear™

Agilus30 is a PolyJet Photopolymer with high tear-resistance, capable of withstanding repeated flexing and bending; thus, it is an ideal material for rapid prototyping and design validation. With a Shore A value of 30 in clear, black and white colorations, the material accurately simulates the look, feel and function of rubber-like products. The Clear version has the best mechanical performance of the series, due to its lack of pigment.

Mechanical Properties	Test Method	Value	
		Black / Translucent	White
Tensile Strength	ASTM D-412	2.4 – 3.1 MPa (348 – 450 psi)	2.1-2.6 MPa (305 – 377 psi)
Elongation at Break	ASTM D-412	220 – 270%	185 – 230%
Compressive Set	ASTM D-395	6 – 7%	6 – 7%
Tensile Tear Resistance	ASTM D-624	4 – 7 Kg/cm (22 – 39 lb/in)	4 – 7 Kg/cm (22 – 39 lb/in)
Other	**Test Method**	**Value**	
		Black / Translucent	White
Shore Hardness	ASTM D-2240	30 – 35 Scale A	30 – 40 Scale A
Polymerized Density	ASTM D-792	1.14 – 1.15 g/cm^3	1.14 – 1.15 g/cm^3

Figure 2.16: Technical information about Agilus30 material.

GelMatrix™

GelMatrix material is, as the name suggest, a very soft gel-like material usually utilized in applications mimicking vascular tissue. In [78], 3D printed arteries demonstrated accurate physiological distensibility values similar to human vessels.

SUP706B™

In addition to the model material selected, the 3D printer offers two options for the support material: SUP705, removable with WaterJet, and SUP706, which is easy to remove and soluble for post-processing automated and greater freedom of geometric design, for print parts with complex and delicate and small cavities. The support material printed along with the models to be tested is called SUP706B™. It is a soluble support suited for hands-free removal with alkaline cleaning solution or mechanical removal by hand or waterjet technology.

After the printing process, the majority of the support material around the pieces was removed manually with the help of some tools (figure 2.17) and then every piece was accurately cleansed with water and an alcoholic solution.

Figure 2.17: Support material removal process.

VeroWhite™

The Vero™ family includes a collection of rigid design materials. These multi-purpose materials are most widely used for visual models, engineering prototypes, product assemblies and RTV molding patterns. Rigid materials like these are also a good choices for light functional testing, patterns, prototypes and models. The VeroWhite material possesses a Young Modulus of $2500MPa$ and a Poisson Ratio of 0.38

For the anatomical-prototype testing, the anatomical support were printed with VeroWhite material (figure 2.18) rather than BoneMatrix. This is because, even thought the models were designed to resemble a part of the femur and tibia geometries, their mechanical properties were not meant to be tested in this study. Another reason for this choice is that in a FEA the stiffness of the bone is extremely higher than the cartilage one. To put in simple words, both printed and computational models of the bones were used mostly for their geometrical and force transmission characteristics, rather than their mechanical behaviour that was considered to be enough rigid for the scope.

Figure 2.18: Printed anatomical supports and femoral cartilage from subject 18 (Degenerative).

2.5 Mechanical Testing

After the advanced additive manufacturing process was completed, all the printed models were brought to Tæknisetur (IceTec) company for the mechanical characterization. Each one of the three test setups that are going to be described below, were performed with the use of the MTS Insight™ (Electromechanical - 10k Standard Length) testing system. The electromechanical load frames have a rectangular shape and include a base unit and one or two vertical columns. The two-column models have a fixed upper transverse beam. The moving crosshead is driven by precision ball screws on the load frame and it is the moving and force generating component during setup and testing.

TestWorks 4 is the MTS Systems Corporation's testing software used in conjunction with the MTS Insight frame system. The software has various method templates available. For example, it provides five basic tensile method templates to help the user create specific tests for your specimens. TestWorks 4 also supplies three compression method templates, allowing the user to configure specific compression procedures. Although the software provides an option to visualize raw data, those were just extracted and uploaded on *Matlab* software, in order to ensure a better control over the post-processing phase.

Except for the *anatomy specific* tests, all the others ones were conducted by following the instructions from the normative related to the specimen tested. Together, ASTM D695 and ASTM D638 assess the fundamental material properties of polymers that are found in every industry and even every household around the globe. Thanks to the materials tested being isotropic, 5 samples of each material were considered enough for each testing setup, according to the ASTM standards.

2.5.1 Tensile test

ASTM D638 is the most common testing standard for determining the tensile properties of reinforced and non-reinforced plastics ASTM D638 is performed by applying a tensile force to a sample specimen and measuring various properties of the specimen under stress. It is conducted on a universal testing machine (also called a tensile testing machine) at tensile rates ranging from 1 to 500 mm/min until the specimen fails (yields or breaks). The most commonly tested shape is a die cut C dogbone specimen, which calls for an overall length of 115 mm (the gauge length being 25 mm), width of 6 mm, and thickness of 3 mm. All specimens must be measured before testing in accordance with ASTM D5947. Thickness of the specimen must be measured three times, with the median value being the accepted value.

In order to test properly, specimens must be held perpendicular to the jaw faces and not tilted on an angle. Specimen misalignment can cause major variations in test results, and proper care should be taken to ensure that the specimens are all aligned consistently for each test. One way of addressing misalignment is by using a jaw face that is close to the same width as the specimen, making it relatively easy to visually adjust alignment. Once grips are tightened onto the specimens in preparation for running a test, unwanted compressive forces are frequently applied. These forces, although minute, can interfere with test results if not treated properly. It is important that they not be balanced after the specimen is inserted, as this will cause an offset in results. A consistent and uniform pressure across the jaw faces ensures that thinning samples do not slip out of the grips during testing.

Ten dogbone specimens were tested for tension using ASTM D638, five made of *soft cartilage* and five of *medium cartilage* materials (figure 2.19).

Figure 2.19: Tensile test on a dogbone specimen.

2.5.2 Compression test

ASTM D695 is a test method used to determine the compressive properties of un-reinforced and reinforced plastics. It is used alongside its tensile test standard equivalent, ASTM D638. ASTM D695 obtains the properties of a material's compressive strength, compressive yield point, and modulus.

Figure 2.20: Compression specimen right before testing.

The standard specimen for strength determination is a right cylinder or prism whose length is twice its principal width or diameter. Specimens can either be blocks or cylinders. We chose the latter: for ASTM, the typical cylinders are 12.7mm in diameter and 25.4mm long. The specimen is placed between and aligned at the very center of the compressive plates, parallel to the surface. The crosshead is adjused until it makes contact with the compression fixture. The specimen is then compressed until failure at a uniform rate in the longitudinal direction. The standard 10k N load cell was used in this case.

Ten cylindrical specimens were tested for compression using ASTM D695, five made of *soft cartilage* and five of *medium cartilage* materials (figure 2.20).

2.5.3 Anatomy specific test

Since the aim of this study was to prototype a mechanical test for femoral cartilage with patient specific anatomical morphology, no specific normative has been followed. The femur and tibia were designed and printed with a geometrical shape that served as a grip site for the jaw faces. This was not part of the original anatomical morphology of the bones, but was added in order to guarantee a proper grip and stability during the testing phase.

The tests were conducted using jaws rather than plates, even though they are typically used for tensile tests. This was possible thanks to the fact that the software is able to extract different measurements from the testing system, permitting thus to customize the collection of data.

Figure 2.21: Anatomy specific testing setup.

Before the test, every cartilage was measured with a digital caliber in six different points: two for the width and four for the thickness. Both femur and tibia were fixed and the jaws were positioned to keep the cartilage perfectly between them and adherent to the femur, as in a physiological

condition (figure 2.21). To secure the positioning, a preload of $650N$ was applied to the cartilage. This choice also has a, more important, physiological justification since the loads acting on the knee joint (for a leg in full-extension position) during the standing phase of the gait cycle range from $700N$ to $1150N$ on average (see *Paragraph 1.1.2*). Starting from there, the compressive load on the cartilage was increased at a uniform rate along the longitudinal direction, until a 20% strain of the total average thickness was reached. After that, the jaws were separated and the cartilages were took to repeat the same measurements described above.

This procedure was carried out for both two subjects/morphologies, with five soft cartilages and five medium cartilages each.

Chapter 3

Data Analysis

3.1 Mechanical tests results

All the data from the mechanical tests performed at Tæknisetur (IceTec) were directly collected from the testing system and then uploaded on Matlab software for the post-processing phase. This applies to the standardized tensile and compression tests performed on the specimens and also to the patient-specific anatomical test design during the study. The most notable results are showed in the following paragraphs and will be discussed in detail in the next chapter.

3.1.1 Stress-strain curves

Here are reported the graphs representing the relation between stress and strain of soft and medium material. The curves from both compression and tensile tests were extrapolated and plotted, in order to have an all-around overview of the behaviour of the materials.

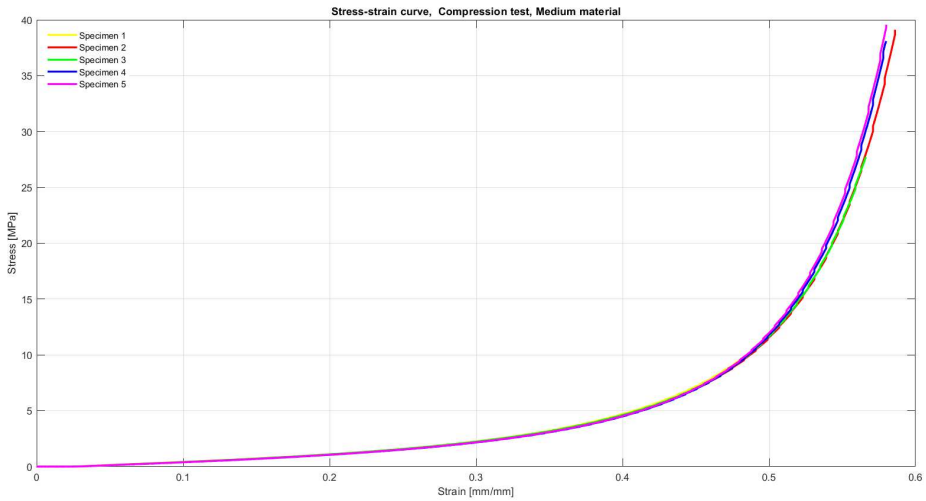

Figure 3.1: Stress-strain curve, Compression test, Medium material.

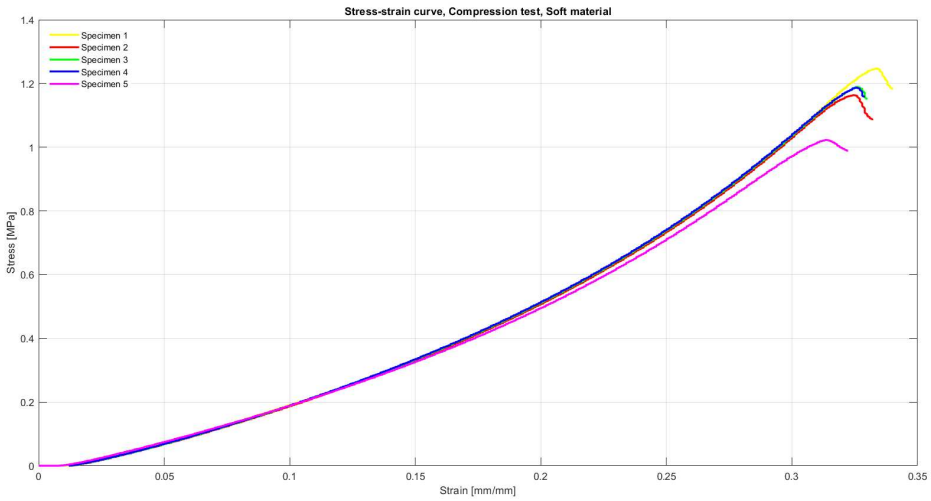

Figure 3.2: Stress-strain curve, Compression test, Soft material.

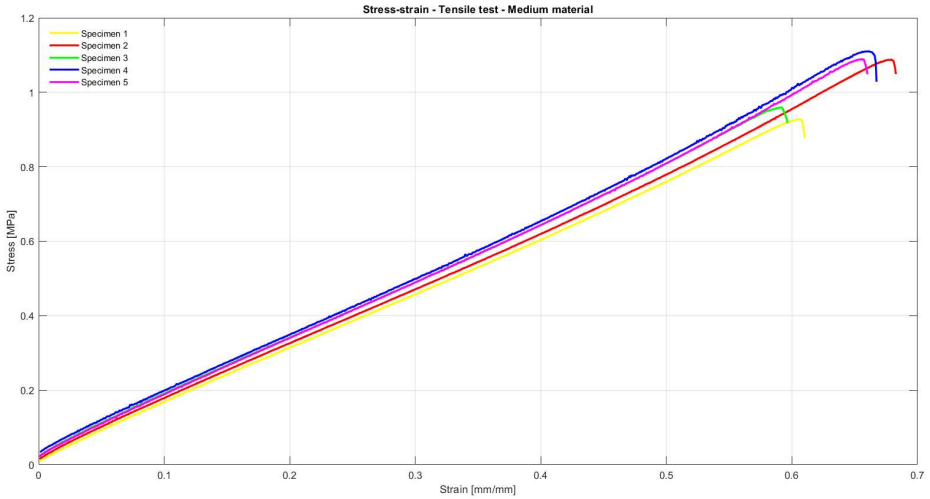

Figure 3.3: Stress-strain curve, Tensile test, Medium material.

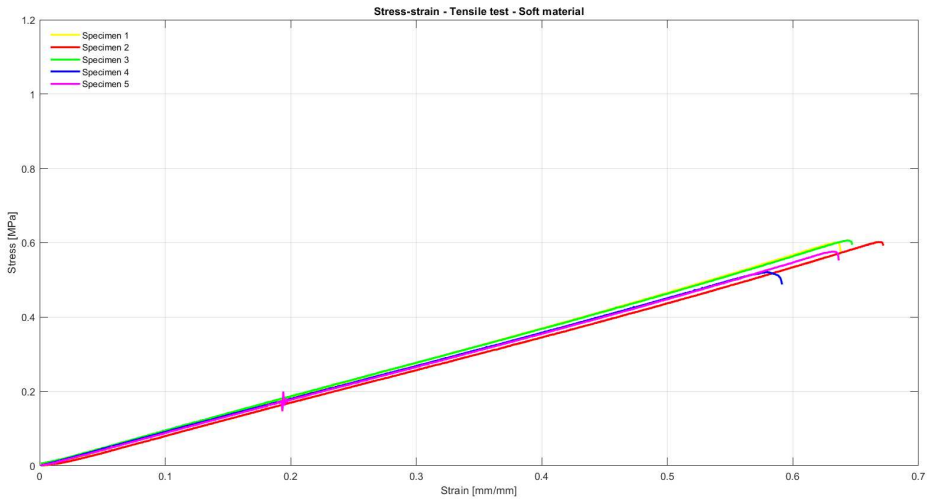

Figure 3.4: Stress-strain curve, Tensile test, Soft material.

3.1.2 Young's Modulus

	Compression	Tension
Medium material	7.2396	1.8377
Soft material	2.4317	0.8784
Native tissue	5	12

Table 3.1: Young's Modulus of printed materials and natural cartilage (from literature), expressed in MPa $[N/mm^2]$

Following ASTM-D695 Standard, the compression modulus of elasticity (Young's) was calculated by drawing a tangent line to the initial linear portion of the load-deformation curve, selecting any point on this straight line portion, and dividing the compressive stress represented by this point by the corresponding strain, measure from the point where the extended tangent line intersects the strain-axis (figure 3.5). The stress-strain curves for medium material were fitted using a 2nd degree exponential fit ($y = a * exp(b * x) + c * exp(d * x)$) with $R\text{-}square = 0.9998$ and $RMSE = 0.1047$. For the soft material, a 4th degree polynomial fit ($f(x) = p1 * x^4 + p2 * x^3 + p3 * x^2 + p4 * x + p5$) was chosen, with $R\text{-}square = 0.999$ and $RMSE = 0.01188$.

The tensile elastic modulus was not important for the final validation of the model but was still calculated to guarantee a more complete insight of the mechanical performances of the printed materials. It was calculated by following the instructions reported on ASTM-D638 standard test method.

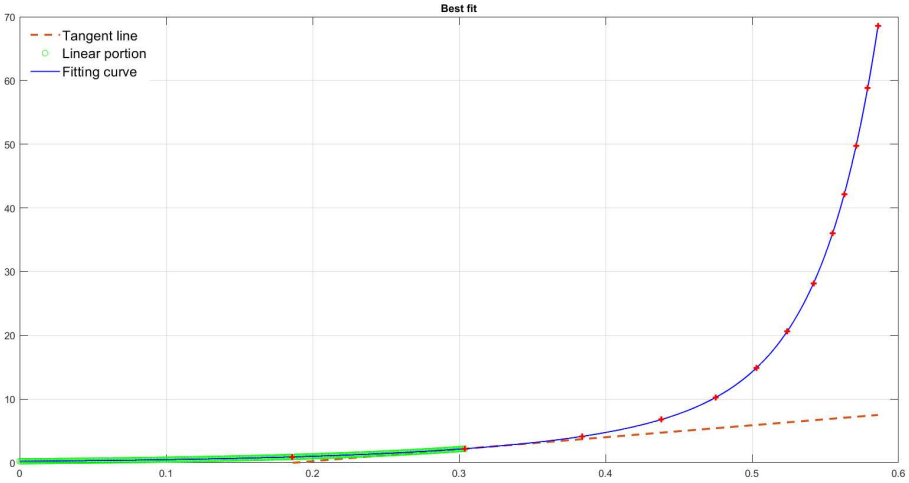

Figure 3.5: Fitted stress-strain curve of compression test on medium material.

3.1.3 Poisson's Ratio

	Poisson's Ratio
Medium material	0.3451
Soft material	0.3462
Native tissue	0.46

Table 3.2: Poisson's Ratio of printed materials and natural cartilage (from literature), expressed as a dimensionless value

The Poisson's ratio was not directly calculated from test parameters, because no extensometers were utilized during the tensile tests. Thus, from the geometry of the specimen, the transversal strain was calculated as follows:

$$\frac{d_0}{w_0} = \alpha \tag{3.1}$$

where:
d_0 = initial depth of the specimen
w_0 = initial width of the specimen

$$d_0 = \alpha * w_0$$

$$V_0 = A_0 * l_0 = w_0 * d_0 * l_0 \tag{3.2}$$

where:
V_0 = initial volume of the specimen
l_0 = initial length of the specimen

$$V_0 = \alpha * w_0^2 * l_0 \tag{3.3}$$

At this point, an assumption about the stress and strain having a linear relation was made. And, considering the volume of the specimen to be conserved during the test (until the break-point), we got:

$$V = \alpha * w^2 * l \tag{3.4}$$

Where the parameters without the 0-subscript signify that we are taking into account a random instant during the test. Then, it was possible to calculate the Δd from the (3.4):

$$w = \sqrt{\frac{V_0}{\alpha * l}} \tag{3.5}$$

And consequently, the transversal strain:

$$\epsilon_t = \frac{w - w_0}{w_0} = \frac{\Delta w}{w_0} \tag{3.6}$$

After that, the Poisson's Ratio was determined by following the instructions reported on ASTM-D638 Standard, for both medium and soft materials. For those materials where there is proportionality of stress to strain and it is possible to determine a modulus of elasticity, a straight line is drawn through each set of points within the load range used for determination of modulus, and the slopes $d\epsilon_a/dP$ and $d\epsilon_t/dP$ of those lines are determined (figure 3.2). Poisson's Ratio is then calculated as follows:

$$|\nu| = \frac{d\epsilon_t/dP}{d\epsilon_a/dP} \tag{3.7}$$

where:

$d\epsilon_t$ = change in transverse strain

$d\epsilon_a$ = change in longitudinal strain

dP = change in applied load

The errors that are introduced by drawing a straight line through the points are reduced by applying the least squares method.

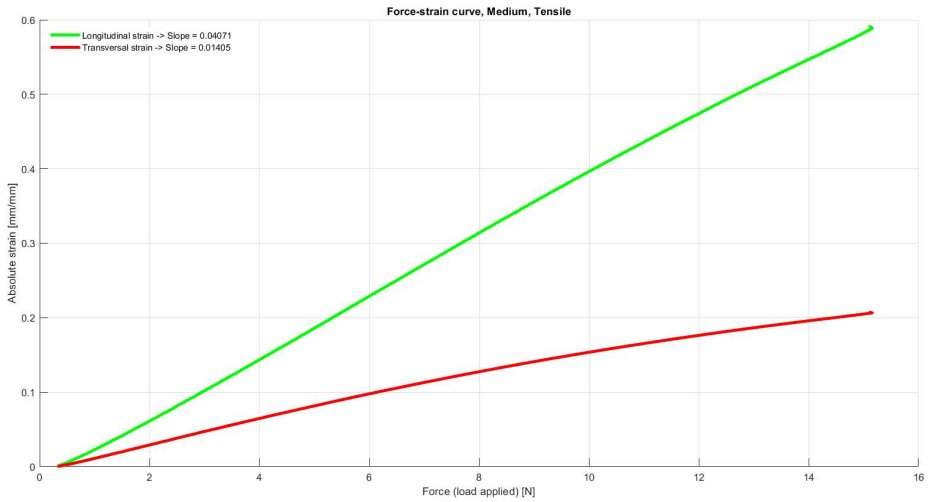

Figure 3.6: Force-strain curve of medium material, utilized to calculate the Poisson's Ratio.

3.1.4 Force-displacement curves

In this section are reported the graphs related to the anatomy-specific testing setup that was prototyped during this study. The force-displacement relation was chosen as it allows for an intuitive understanding of the test's trend and thus it leads to a direct comparison with the computational results for the final model validation.

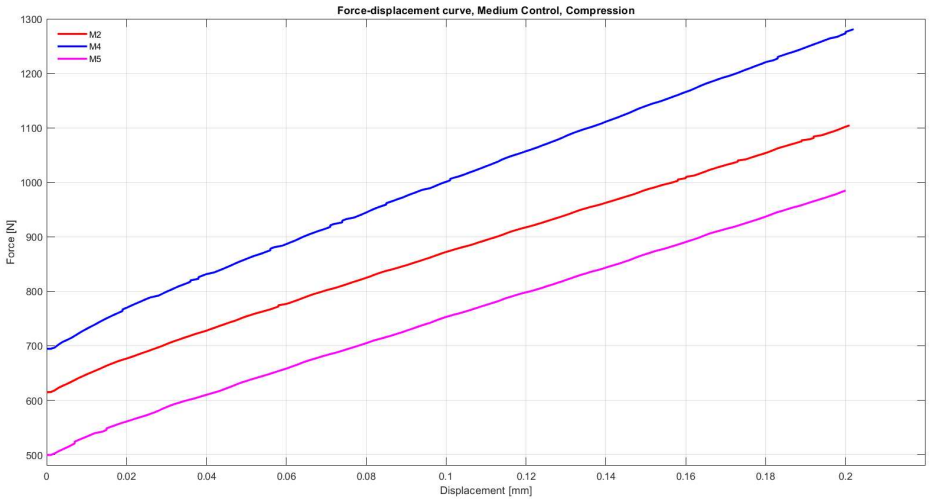

Figure 3.7: Force-displacement curve of medium material with control subject morphology.

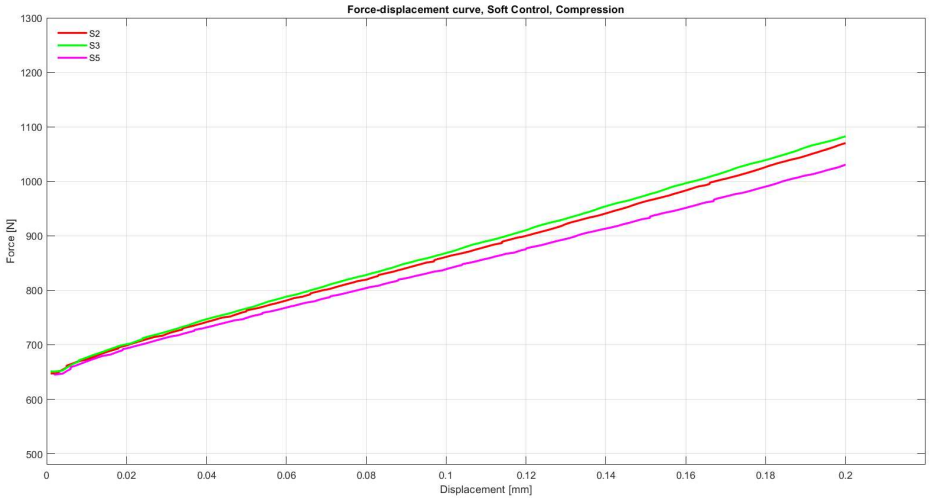

Figure 3.8: Force-displacement curve of soft material with control subject morphology.

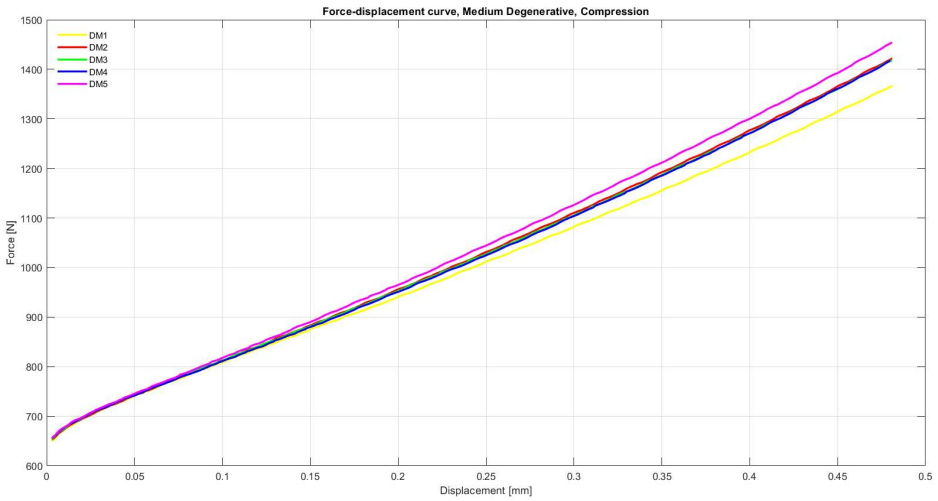

Figure 3.9: Force-displacement curve of medium material with degenerative subject morphology.

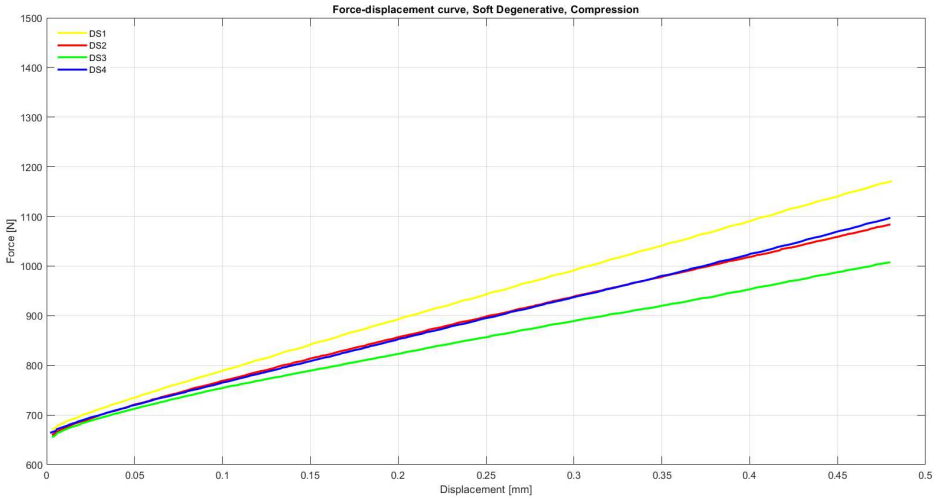

Figure 3.10: Force-displacement curve of soft material with degenerative subject morphology.

3.2 Computational tests results

In this section are reported the graphical and numerical results of the computational analysis described in *Paragraph 2.3*. This data serve as a comparison and validation for the data extracted from the mechanical tests showed in the previous paragraph.

3.2.1 Force-displacement curves

Force-displacement curves were again chosen in order to have a parameter of comparison with the mechanical tests with patient-specific anatomical supports.

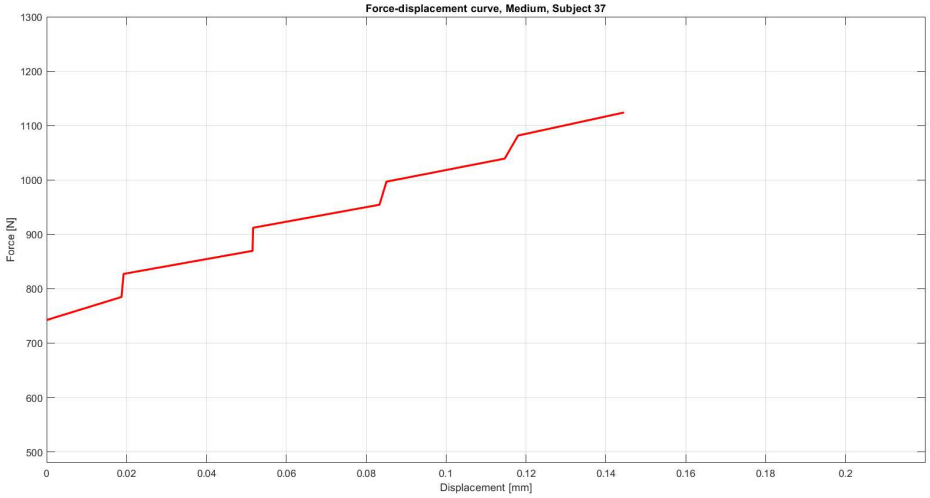

Figure 3.11: Force-displacement curve of Medium material with control subject morphology.

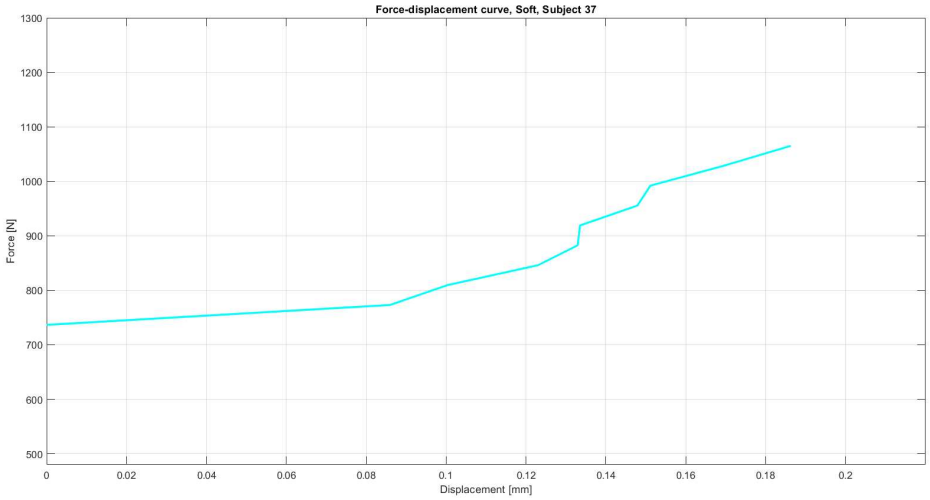

Figure 3.12: Force-displacement curve of soft material with control subject morphology.

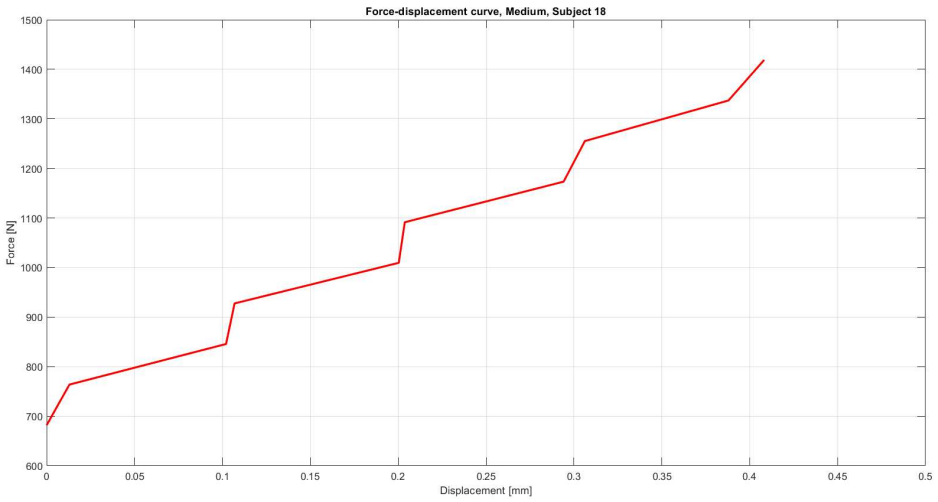

Figure 3.13: Force-displacement curve of medium material with degenerative subject morphology.

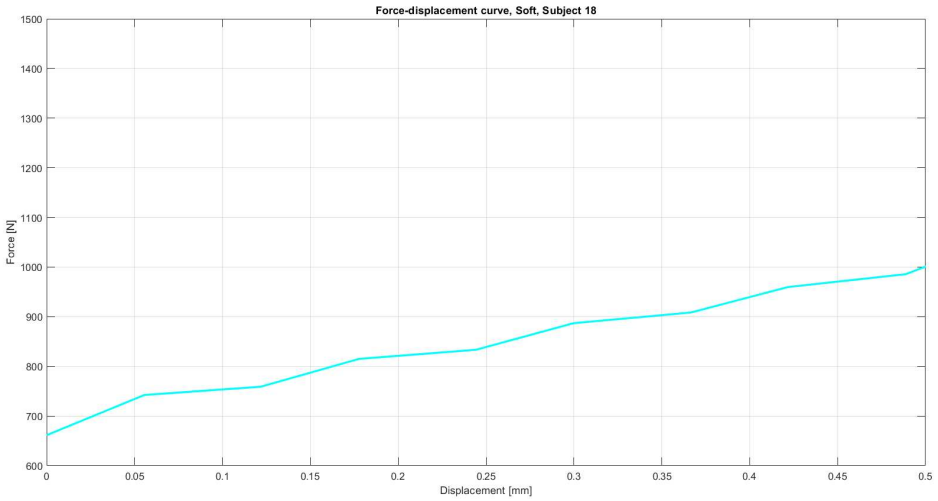

Figure 3.14: Force-displacement curve of soft material with degenerative subject morphology.

3.2.2 Equivalent strain distribution

The model's results considered useful for the purpose of this study were mainly the Equivalent von Mises stress and Equivalent von Mises strain. The von Mises stress, which accounts for both the normal and shear loads that are acting on the material, is a measurement of the equivalent or effective stress in a material. The von Mises strain, on the other hand, accounts for both normal and shear strains acting on a material and is a measurement of the equivalent or effective strain in a material.

In order to give a better understanding of how the model can predict physiological conditions, a computational test with cartilage having material properties from literature was carried out. The graphic and numerical results are shown in the following pictures.

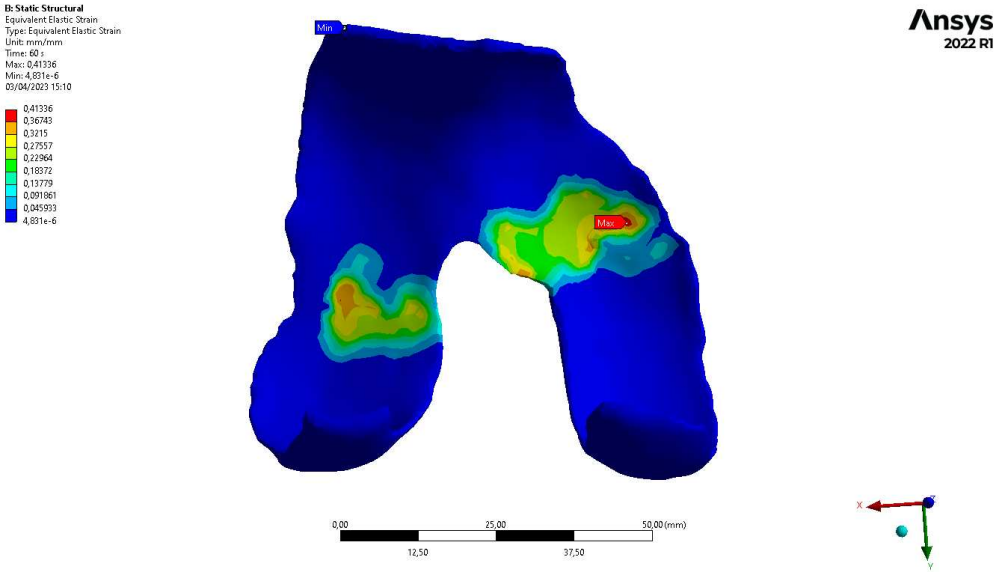

Figure 3.15: Strain distribution on subject 37, Medium material properties.

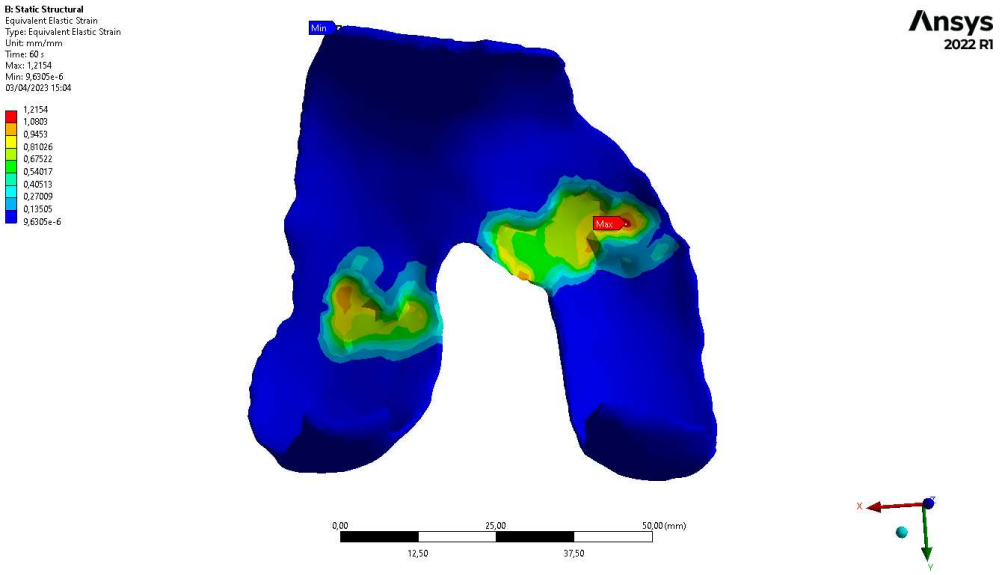

Figure 3.16: Strain distribution on subject 37, Soft material properties.

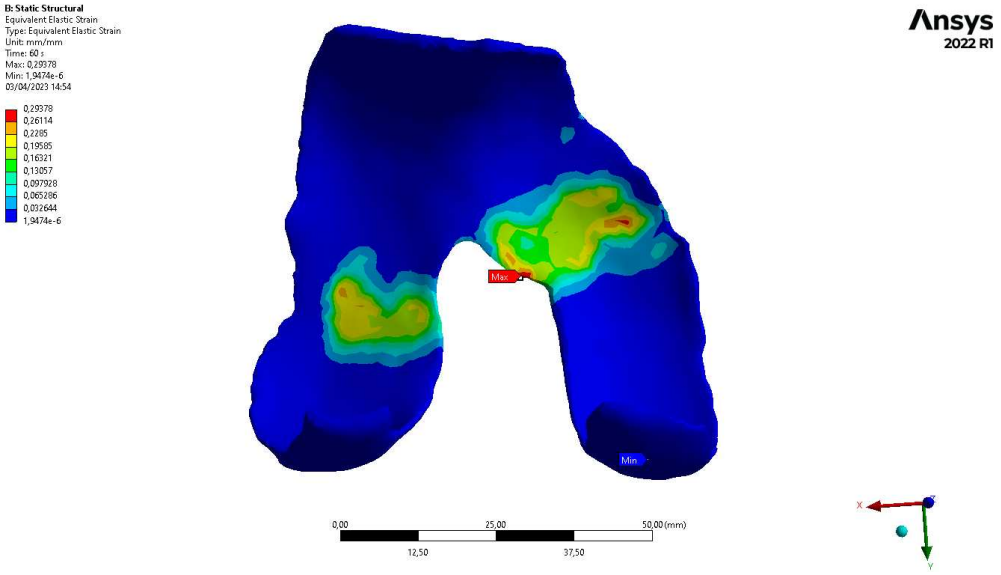

Figure 3.17: Strain distribution on subject 37, Literature material properties.

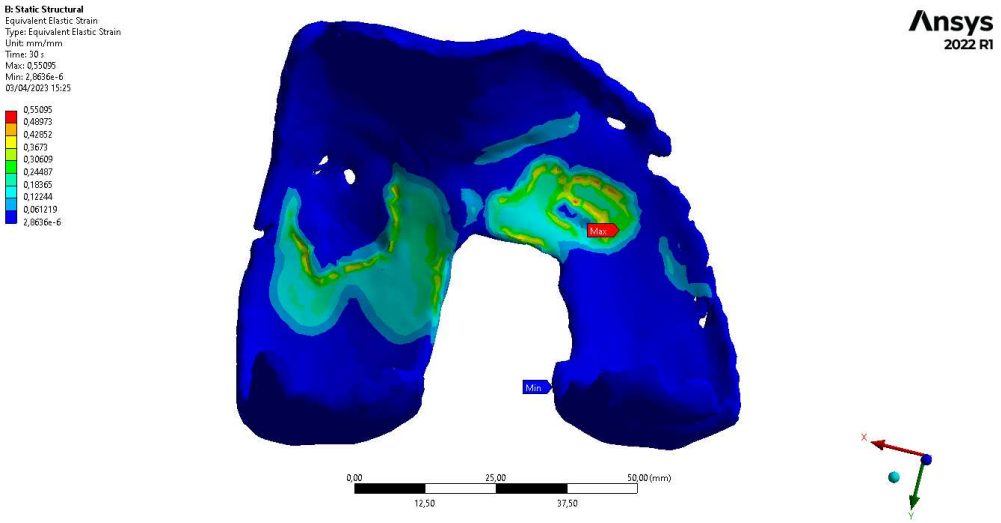

Figure 3.18: Strain distribution on subject 18, Medium material properties.

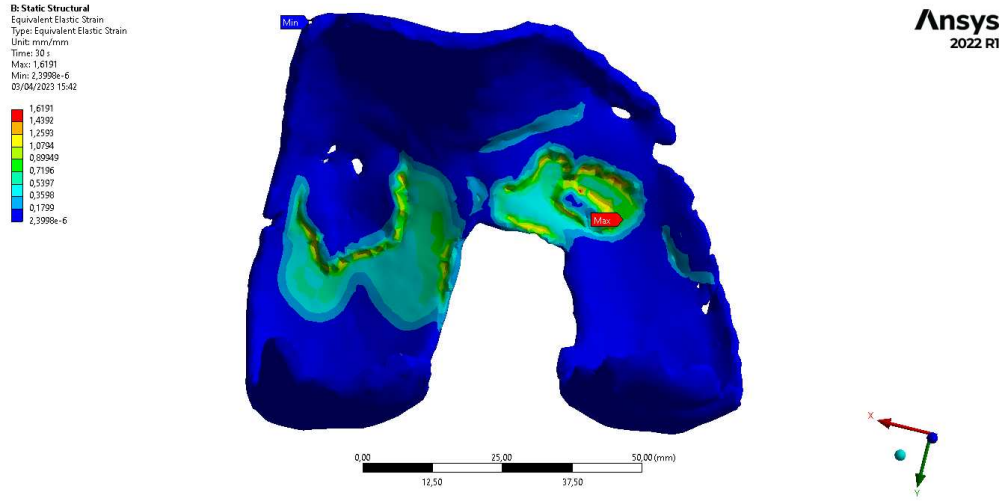

Figure 3.19: Strain distribution on subject 18, Soft material properties.

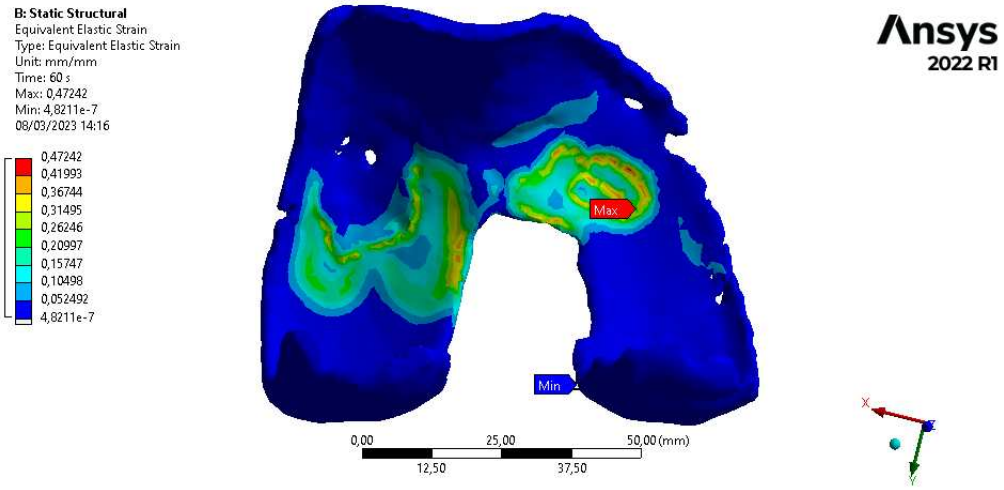

Figure 3.20: Strain distribution on subject 18, Literature material properties.

Chapter 4

Results Discussion

4.1 Printed materials

4.1.1 Specimens results

For what concerns the compression performance, the materials exhibit a similar behaviour by comparing the very first part of the medium curve (figure 3.1) with the whole soft curve (figure 3.2), until the breakpoints. But making a comparison by taking into account the whole medium curve, shows that the materials have a quite different compressive behaviour, with the medium reaching stresses an order of magnitude bigger. However, this could also be due to the inability of reaching a breakpoint for the medium material cylindrical specimens.

The tensile behaviour of the two materials (soft and medium) is approximately linear for both, with the medium reaching higher peaks of stress (figure 3.3) as expected. In particular, they have a breakpoint that does not go past 0.7 mm/mm but the soft almost reaches 0.6 Mpa (figure 3.4), which, on average, is half of the maximum stress reached by the medium material with almost 1.2 Mpa. This suggests that there might be a linear relation between the tensile behaviours of the two materials.

4.1.2 Parameters results

The elastic (Young's) modulus is a measurement of a material's resistance to elastic deformation, when stress is applied to it. For instance, the higher the modulus is, the stiffer the material. And this can be easily seen in our results as well, since the modulus of the medium material is even three times higher than that of the soft one. This matches the initial expectations, but what's curious is that the modulus of the native cartilage tissue (on average, from literature) stands in between. It is rather important to notice that the mechanical performance of biological cartilage tissue is affected by a lot of factors (i.e. age, OA, physical activity) and thus it's difficult to discriminate a standard mechanical performance. For this reason, the results from printed materials could be considered the extreme points of a range of values, with the soft being the lower limit (i.e. osteoarthritic cartilage) and the medium being the upper limit (i.e. healthy cartilage).

Poisson's ratio is another elastic parameter and defines the relation between longitudinal and transversal strain. It ranges from 0 to 0,5, with the latter meaning that the material is virtually incompressible. Both materials exhibit a similar Poisson's ratio and this could be due to the fact that they also shows a linear behaviour when it comes to tensile performance (for instance, it is useful to remember that the Poisson's ratio is calculated from tensile tests parameters). The native cartilage tissue has a ratio usually ranging from 0.45 to 0.47, making it almost incompressible and quite higher then its printed counterparts. However, the biological components of the tissue play

a major role in lowering its compressibility and it was not possible to replicate their effect in this study, so this could explain the gap between biological and synthetic performance.

4.1.3 Anatomy-specific results

The curve behaviour is comparable to what expected from the extrapolated parameters (elastic modulus and Poisson's ratio). The medium material is stiffer and thus a higher applied load is needed in order to reach the 20% of deformation, compared to its soft counterpart; this applies for both control and degenerative morphologies, despite having different thicknesses and thus requiring more load in general to reach the deformation needed. This serves also as a demonstration of how the morphology of the specific cartilage influences the load condition/distribution. For instance, degenerative OA cartilage tissue has been reported [60] to have an increased volume (and, consequently, thickness) due to swelling of the tissue, compared to the healthy physiological condition.

However, this results will become more significant when compared to the computational simulation outcome, in the next paragraph.

4.2 Finite element simulation

Before comparing computational curves with the ones from mechanical tests, is worth to point out that the finite element analysis results are evaluated with far less data. This leads to less linear curves and thus that's why the focus is mostly for the average trend and the max values.

For the control subject, it is straightforward to notice that the computational force-displacement curves do not match the ones from mechanical test properly. Both soft and medium curves have similar trends (this is more true for the medium material) but they do not reach the same max forces and displacements.

On the other hand, degenerative subject results show a very close match between the two approaches. The computational curves do not only exhibit the same trend as the ones from mechanical testing, but they also have just slightly lower maximum values for both stress and strain. This applies to the medium and the soft material as well.

This means that the degenerative cartilage is more suited to be implemented in this kind of parallel approach. And, in general, this leads to the conclusion that having a wider interacting surface on the model is an important point in order to have comparable results.

4.3 Qualitative comparison

These pictures serves as a qualitative comparison between zone subjected to major strains on the cartilage surface. On the left of each picture, the printed cartilages after their respective mechanical tests. On the right side, the corresponding cartilage from the computational analysis.

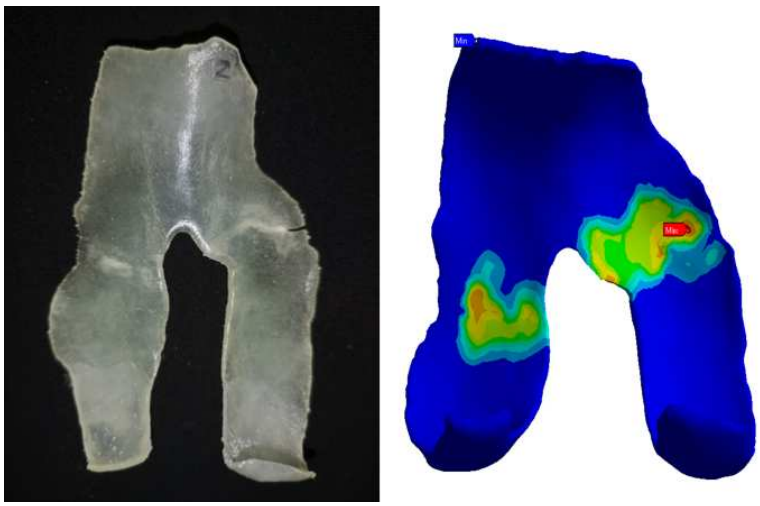

Figure 4.1: Comparison on subject 37, Medium material properties.

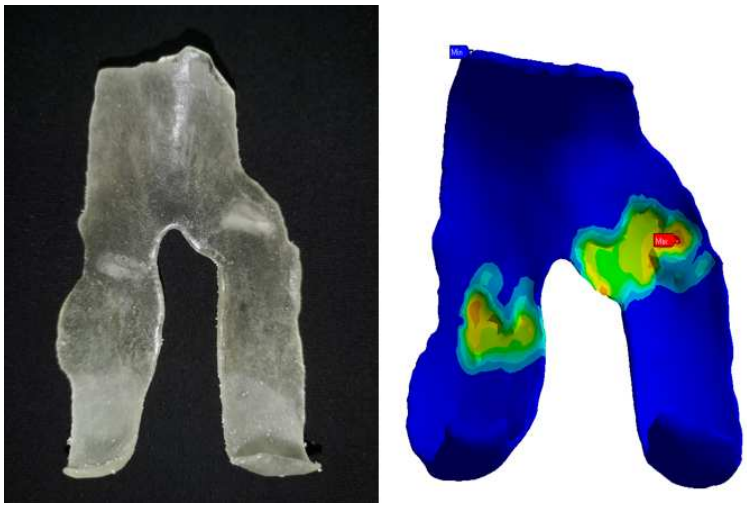

Figure 4.2: Comparison on subject 37, Soft material properties.

For the subject 37 (control) it is easier to appreciate the zones were the strain reaches its maximum. This could be due to the cartilage model being thinner on average. In particular, it is interesting to notice that for the medium material (Figure 4.1) the max strain value on the computational one, corresponds to the exact point were the printed one broke. This is a promising result to understand if this approach could be able to predict zones were the rupture of cartilage would eventually occur.

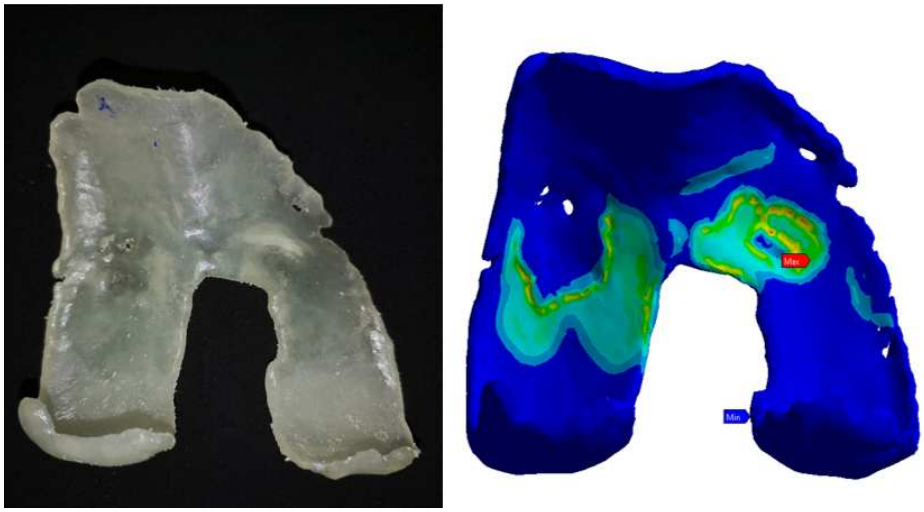

Figure 4.3: Comparison on subject 18, Medium material properties.

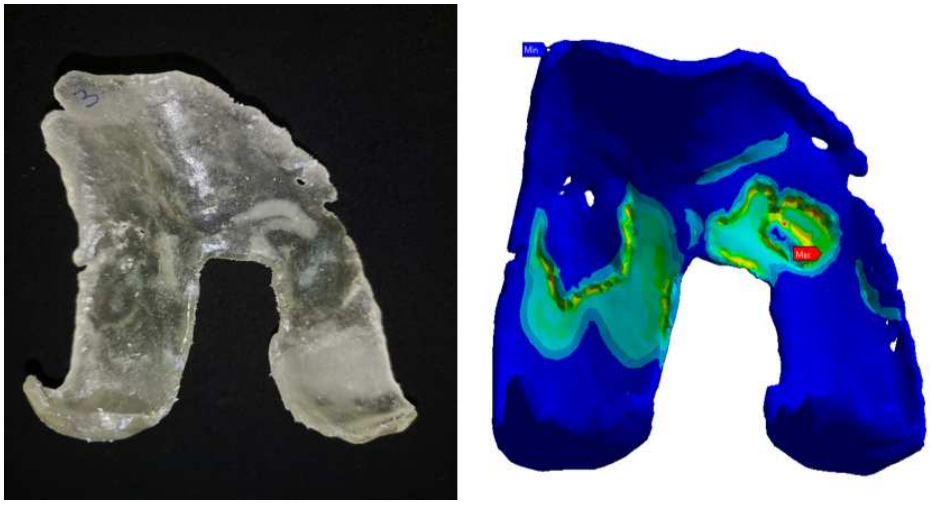

Figure 4.4: Comparison on subject 18, Soft material properties.

In the subject 18 model, it is slightly more difficult to appreciate the peak strains, due to the fact that the strain is more diffused on the surface of the cartilage.This could be because of the subject more voluminous (due to swelling of native tissue) morphology and thus more contact area with the bone. However, it is still possible to observe a resemblance in the most deformed zones of both surfaces.

Conclusion

In the frame of this project, two parallel approaches leading to several conclusions and results were carried out. The tensile and compression tests performed on standardized samples led to encouraging results for the compression modulus. The native tissue has a modulus that is, on average, comprised between the two digital anatomy materials. This means that by adjusting the mixture of materials it could be possible to reach the same value of native tissue.

Speaking of the validation of patient-specific prototype mechanical test, the computational results are satisfying for the degenerative morphology. The curves for both approaches exhibit greatly comparable results in terms of trend of the curve and maximum stress/strain. This serves as a proof that the designed prototype of testing setup has the potential to be studied as a predicting tool for loads and deformations acting on the articular cartilage. In an ideal approach, this could allow for predictions of zones were a chondral defect could possibly form in case of osteoarthritis.

Confirming this even more are the visual comparisons of the most deformed zones on cartilage models, printed and computational.

Limitations encountered

First of all, some results were not significative for the purpose of this study. Those includes the tensile elastic modulus of the printed material, that showed poor comparability with its native counterpart. But also the force-displacement curves of control subject from FEA were not useful in the validation of the testing setup.

Another major limitation is the biomechanical behaviour of the native cartilage, being biphasic poroviscoelastic, but here assumed as linear isotropic elastic. However, in a lot of studies this was acceptable if we consider only the instant deformation of the tissue. Beside of the constitutive model, it is rather difficult for a synthetic material to emulate the biological composition and structure of a native human tissue.

The choice of studying two different morphologies (control and degenerative) was taken in order investigate whether osteoarthritis effect could influence this tests, for both approaches. The results do not shows particular insights on the relevance of the morphology. The only notable point is that a cartilage with bigger volume (area and thickness) offers more reliable and replicable results.

Future developments

In the end, it is worth to remember that Polyjet technique in combination with Digital Anatomy Printing still offers many possibilities to be explored. This was a first approach, but by changing the mixture of digital materials it could be possible to achieve a mechanical performance more and more close to that of the native articular cartilage.

The prototype testing setup still has to be fully validated, but results could be interesting in terms of predicting cartilage failure. This is crucial in a field were there is a shortage of tissue samples for testing and were the replicability is not usually guaranteed. Moreover, the typical testing methods focus on the mechanical characterization only, not taking into account the

mophology and geometrical structure of the tissue. One of the limitations was the simplification of the model from an anatomical point of view. This could be overcome in the future by adding muscles, ligaments and menisci.

In the healthcare field, were the future directions point toward the patient-specific approach, 3D modeling and printing offer a wide and increasing variety of solutions for specialist.

Bibliography

[1] S. Amin, N. Luepongsak, C. A. McGibbon, M. P. LaValley, D. E. Krebs, and D. T. Felson, "Knee adduction moment and development of chronic knee pain in elders," *Arthritis care & research*, vol. 51, no. 3, pp. 371–376, 2004.

[2] D. T. Felson, Y. Zhang, M. T. Hannan, A. Naimark, B. Weissman, P. Aliabadi, and D. Levy, "Risk factors for incident radiographic knee osteoarthritis in the elderly. the framingham study," *Arthritis & Rheumatism: Official Journal of the American College of Rheumatology*, vol. 40, no. 4, pp. 728–733, 1997.

[3] F. W. Roemer, Y. Zhang, J. Niu, J. A. Lynch, M. D. Crema, M. D. Marra, M. C. Nevitt, D. T. Felson, L. B. Hughes, G. Y. El-Khoury, *et al.*, "Tibiofemoral joint osteoarthritis: risk factors for mr-depicted fast cartilage loss over a 30-month period in the multicenter osteoarthritis study," *Radiology*, vol. 252, no. 3, pp. 772–780, 2009.

[4] D. T. Felson, J. J. Anderson, A. Naimark, A. M. Walker, and R. F. Meenan, "Obesity and knee osteoarthritis: the framingham study," *Annals of internal medicine*, vol. 109, no. 1, pp. 18–24, 1988.

[5] M. Blagojevic, C. Jinks, A. Jeffery, and K. Jordan, "Risk factors for onset of osteoarthritis of the knee in older adults: a systematic review and meta-analysis," *Osteoarthritis and cartilage*, vol. 18, no. 1, pp. 24–33, 2010.

[6] J. Niu, Y. Zhang, J. Torner, M. Nevitt, C. Lewis, P. Aliabadi, B. Sack, M. Clancy, L. Sharma, and D. Felson, "Is obesity a risk factor for progressive radiographic knee osteoarthritis?," *Arthritis Care & Research*, vol. 61, no. 3, pp. 329–335, 2009.

[7] L. Sharma, C. Lou, D. T. Felson, D. D. Dunlop, G. Kirwan-Mellis, K. W. Hayes, D. Weinrach, and T. S. Buchanan, "Laxity in healthy and osteoarthritic knees," *Arthritis & Rheumatism: Official Journal of the American College of Rheumatology*, vol. 42, no. 5, pp. 861–870, 1999.

[8] L. Sharma, J. Song, D. T. Felson, S. Cahue, E. Shamiyeh, and D. D. Dunlop, "The role of knee alignment in disease progression and functional decline in knee osteoarthritis," *Jama*, vol. 286, no. 2, pp. 188–195, 2001.

[9] S. Tanamas, F. S. Hanna, F. M. Cicuttini, A. E. Wluka, P. Berry, and D. M. Urquhart, "Does knee malalignment increase the risk of development and progression of knee osteoarthritis? a systematic review," *Arthritis Care & Research: Official Journal of the American College of Rheumatology*, vol. 61, no. 4, pp. 459–467, 2009.

[10] A. Baliunas, D. Hurwitz, A. Ryals, A. Karrar, J. Case, J. Block, and T. Andriacchi, "Increased knee joint loads during walking are present in subjects with knee osteoarthritis," *Osteoarthritis and cartilage*, vol. 10, no. 7, pp. 573–579, 2002.

[11] L. E. Thorp, D. R. Sumner, M. A. Wimmer, and J. A. Block, "Relationship between pain and medial knee joint loading in mild radiographic knee osteoarthritis," *Arthritis care & research*, vol. 57, no. 7, pp. 1254–1260, 2007.

[12] J. Wong, N. Steklov, S. Patil, C. Flores-Hernandez, M. Kester, C. W. Colwell Jr, and D. D. D'Lima, "Predicting the effect of tray malalignment on risk for bone damage and implant subsidence after total knee arthroplasty," *Journal of Orthopaedic Research*, vol. 29, no. 3, pp. 347–353, 2011.

[13] E. Otten, "Inverse and forward dynamics: models of multi–body systems," *Philosophical Transactions of the Royal Society of London. Series B: Biological Sciences*, vol. 358, no. 1437, pp. 1493–1500, 2003.

[14] J. Morrison, "The mechanics of the knee joint in relation to normal walking," *Journal of biomechanics*, vol. 3, no. 1, pp. 51–61, 1970.

[15] J. Morrison, "Bioengineering analysis of force actions transmitted by the knee joint," *Bio-Med*, vol. 3, pp. 164–170, 1968.

[16] K. E. Wilk, R. F. Escamilla, G. S. Fleisig, S. W. Barrentine, J. R. Andrews, and M. L. Boyd, "A comparison of tibiofemoral joint forces and electromyographic activit during open and closed kinetic chain exercises," *The American journal of sports medicine*, vol. 24, no. 4, pp. 518–527, 1996.

[17] R. Nisell, M. O. Ericson, G. Nemeth, and J. Ekholm, "Tibiofemoral joint forces during isokinetic knee extension," *The American journal of sports medicine*, vol. 17, no. 1, pp. 49–54, 1989.

[18] R. D. Komistek, T. R. Kane, M. Mahfouz, J. A. Ochoa, and D. A. Dennis, "Knee mechanics: a review of past and present techniques to determine in vivo loads," *Journal of biomechanics*, vol. 38, no. 2, pp. 215–228, 2005.

[19] C. R. Winby, D. G. Lloyd, T. F. Besier, and T. B. Kirk, "Muscle and external load contribution to knee joint contact loads during normal gait," *Journal of biomechanics*, vol. 42, no. 14, pp. 2294–2300, 2009.

[20] D. G. Lloyd and T. F. Besier, "An emg-driven musculoskeletal model to estimate muscle forces and knee joint moments in vivo," *Journal of biomechanics*, vol. 36, no. 6, pp. 765–776, 2003.

[21] K. R. Kaufman, K.-N. An, W. J. Litchy, B. F. Morrey, and E. Y. Chao, "Dynamic joint forces during knee isokinetic exercise," *The American journal of sports medicine*, vol. 19, no. 3, pp. 305–316, 1991.

[22] G. E. Lutz, R. Palmitier, K.-N. An, and E. Chao, "Comparison of tibiofemoral joint forces during open-kinetic-chain and closed-kinetic-chain exercises.," *JBJS*, vol. 75, no. 5, pp. 732–739, 1993.

[23] K. B. Shelburne and M. G. Pandy, "A dynamic model of the knee and lower limb for simulating rising movements," *Computer Methods in Biomechanics & Biomedical Engineering*, vol. 5, no. 2, pp. 149–159, 2002.

[24] S. M. Smith, R. A. Cockburn, A. Hemmerich, R. M. Li, and U. P. Wyss, "Tibiofemoral joint contact forces and knee kinematics during squatting," *Gait & posture*, vol. 27, no. 3, pp. 376–386, 2008.

[25] R. D. Komistek, J. B. Stiehl, D. A. Dennis, R. D. Paxson, and R. W. Soutas-Little, "Mathematical model of the lower extremity joint reaction forces using kane's method of dynamics," *Journal of Biomechanics*, vol. 31, no. 2, pp. 185–189, 1997.

[26] A. Seireg and R. Arvikar, "The prediction of muscular load sharing and joint forces in the lower extremities during walking," *Journal of biomechanics*, vol. 8, no. 2, pp. 89–102, 1975.

[27] J. Collins, "The redundant nature of locomotor optimization laws," *Journal of biomechanics*, vol. 28, no. 3, pp. 251–267, 1995.

[28] K. A. Athanasiou, M. Rosenwasser, J. Buckwalter, T. Malinin, and V. C. Mow, "Interspecies comparisons of in situ intrinsic mechanical properties of distal femoral cartilage," *Journal of orthopaedic research*, vol. 9, no. 3, pp. 330–340, 1991.

[29] V. C. Mow and W. M. Lai, "Recent developments in synovial joint biomechanics," *Siam Review*, vol. 22, no. 3, pp. 275–317, 1980.

[30] A. Maroudas, P. Bullough, S. Swanson, and M. Freeman, "The permeability of articular cartilage," *The Journal of bone and joint surgery. British volume*, vol. 50, no. 1, pp. 166–177, 1968.

[31] V. C. Mow, M. H. Holmes, and W. M. Lai, "Fluid transport and mechanical properties of articular cartilage: a review," *Journal of biomechanics*, vol. 17, no. 5, pp. 377–394, 1984.

[32] D. Eyre, "The collagens of articular cartilage," in *Seminars in arthritis and rheumatism*, vol. 21, pp. 2–11, Elsevier, 1991.

[33] N. Broom, "Further insights into the structural principles governing the function of articular cartilage.," *Journal of anatomy*, vol. 139, no. Pt 2, p. 275, 1984.

[34] W. Hwang, B. Li, L. Jin, K. Ngo, N. Schachar, and G. Hughes, "Collagen fibril structure of normal, aging, and osteoarthritic cartilage," *The Journal of pathology*, vol. 167, no. 4, pp. 425–433, 1992.

[35] A. Jeffery, G. Blunn, C. Archer, and G. Bentley, "Three-dimensional collagen architecture in bovine articular cartilage," *The Journal of bone and joint surgery. British volume*, vol. 73, no. 5, pp. 795–801, 1991.

[36] R. Teshima, T. Otsuka, N. Takasu, N. Yamagata, and K. Yamamoto, "Structure of the most superficial layer of articular cartilage," *The Journal of bone and joint surgery. British volume*, vol. 77, no. 3, pp. 460–464, 1995.

[37] J. C. Rousseau and P. Garnero, "Biological markers in osteoarthritis," *Bone*, vol. 51, no. 2, pp. 265–277, 2012.

[38] P. Manninen, H. Riihimäki, M. Heliövaara, and P. Mäkelä, "Overweight, gender and knee osteoarthritis.," *International journal of obesity and related metabolic disorders: journal of the International Association for the Study of Obesity*, vol. 20, no. 6, pp. 595–597, 1996.

[39] V. Valderrabano, V. Von Tscharner, B. M. Nigg, B. Hintermann, B. Goepfert, T. S. Fung, C. B. Frank, and W. Herzog, "Lower leg muscle atrophy in ankle osteoarthritis," *Journal of orthopaedic research*, vol. 24, no. 12, pp. 2159–2169, 2006.

[40] J. A. Buckwalter, J. A. Martin, and T. D. Brown, "Perspectives on chondrocyte mechanobiology and osteoarthritis," *Biorheology*, vol. 43, no. 3-4, pp. 603–609, 2006.

[41] M. J. Benito, D. J. Veale, O. FitzGerald, W. B. Van Den Berg, and B. Bresnihan, "Synovial tissue inflammation in early and late osteoarthritis," *Annals of the rheumatic diseases*, vol. 64, no. 9, pp. 1263–1267, 2005.

[42] M. B. Hurtig, M. D. Buschmann, L. A. Fortier, C. D. Hoemann, E. B. Hunziker, J. S. Jurvelin, P. Mainil-Varlet, C. W. McIlwraith, R. L. Sah, and R. A. Whiteside, "Preclinical studies for cartilage repair: recommendations from the international cartilage repair society," *Cartilage*, vol. 2, no. 2, pp. 137–152, 2011.

[43] J.-P. Berteau, M. Oyen, and S. Shefelbine, "Permeability and shear modulus of articular cartilage in growing mice," *Biomechanics and modeling in mechanobiology*, vol. 15, pp. 205–212, 2016.

[44] A. Maroudas, P. Bullough, S. Swanson, and M. Freeman, "The permeability of articular cartilage," *The Journal of bone and joint surgery. British volume*, vol. 50, no. 1, pp. 166–177, 1968.

[45] V. C. Mow, M. H. Holmes, and W. M. Lai, "Fluid transport and mechanical properties of articular cartilage: a review," *Journal of biomechanics*, vol. 17, no. 5, pp. 377–394, 1984.

[46] V. C. Mow, S. Kuei, W. M. Lai, and C. G. Armstrong, "Biphasic creep and stress relaxation of articular cartilage in compression: theory and experiments," *Journal of biomechanics*, vol. 102, pp. 73–84, 1980.

[47] A. Eberhardt, L. Keer, J. L. Lewis, and V. Vithoontien, "An analytical model of joint contact," 1990.

[48] D. Eyre, "The collagens of articular cartilage," vol. 21, no. 3, pp. 2–11, 1991.

[49] C. Armstrong, W. Lai, and V. Mow, "An analysis of the unconfined compression of articular cartilage," 1984.

[50] G. A. Ateshian, N. O. Chahine, I. M. Basalo, and C. T. Hung, "The correspondence between equilibrium biphasic and triphasic material properties in mixture models of articular cartilage," *Journal of biomechanics*, vol. 37, no. 3, pp. 391–400, 2004.

[51] V. Klika, E. A. Gaffney, Y.-C. Chen, and C. P. Brown, "An overview of multiphase cartilage mechanical modelling and its role in understanding function and pathology," *journal of the mechanical behavior of biomedical materials*, vol. 62, pp. 139–157, 2016.

[52] J. A. Buckwalter, V. C. Mow, and A. Ratcliffe, "Restoration of injured or degenerated articular cartilage," *JAAOS-Journal of the American Academy of Orthopaedic Surgeons*, vol. 2, no. 4, pp. 192–201, 1994.

[53] A. J. Sophia Fox, A. Bedi, and S. A. Rodeo, "The basic science of articular cartilage: structure, composition, and function," *Sports health*, vol. 1, no. 6, pp. 461–468, 2009.

[54] T. D. Brown and A. M. DiGioia III, "A contact-coupled finite element analysis of the natural adult hip," *Journal of biomechanics*, vol. 17, no. 6, pp. 437–448, 1984.

[55] T. D. Brown and A. M. DiGioia III, "A contact-coupled finite element analysis of the natural adult hip," *Journal of biomechanics*, vol. 17, no. 6, pp. 437–448, 1984.

[56] D. Anderson, T. Brown, and E. Radin, "Stress wave effects in a finite element analysis of an impulsively loaded articular joint," *Proceedings of the Institution of Mechanical Engineers, Part H: Journal of Engineering in Medicine*, vol. 205, no. 1, pp. 27–34, 1991.

[57] D. Anderson, T. Brown, K. Yang, and E. Radin, "A dynamic finite element analysis of impulsive loading of the extension-splinted rabbit knee," 1990.

[58] V. Roth and V. Mow, "Finite element analysis of contact problems for indentation of articular cartilage," *Advances in Bioengineering*, pp. 47–48, 1977.

[59] J. E. Hale, M. J. Rudert, and T. D. Brown, "Indentation assessment of biphasic mechanical property deficits in size-dependent osteochondral defect repair," *Journal of biomechanics*, vol. 26, no. 11, pp. 1319–1325, 1993.

[60] F. K. Ciliberti, L. Guerrini, A. E. Gunnarsson, M. Recenti, D. Jacob, V. Cangiano, Y. A. Tesfahunegn, A. S. Islind, F. Tortorella, M. Tsirilaki, *et al.*, "Ct-and mri-based 3d reconstruction of knee joint to assess cartilage and bone," *Diagnostics*, vol. 12, no. 2, p. 279, 2022.

[61] A. Beris, R. Armstrong, and R. Brown, "Perturbation theory for viscoelastic fluids between eccentric rotating cylinders," *Journal of non-newtonian fluid mechanics*, vol. 13, no. 2, pp. 109–148, 1983.

[62] K. D. Brandt, P. Dieppe, and E. L. Radin, "Etiopathogenesis of osteoarthritis," *Rheumatic Disease Clinics of North America*, vol. 34, no. 3, pp. 531–559, 2008.

[63] S. Farrokhi, J. Keyak, and C. Powers, "Individuals with patellofemoral pain exhibit greater patellofemoral joint stress: a finite element analysis study," *Osteoarthritis and Cartilage*, vol. 19, no. 3, pp. 287–294, 2011.

[64] M. Mononen, M. Mikkola, P. Julkunen, R. Ojala, M. Nieminen, J. Jurvelin, and R. Korhonen, "Effect of superficial collagen patterns and fibrillation of femoral articular cartilage on knee joint mechanics—a 3d finite element analysis," *Journal of biomechanics*, vol. 45, no. 3, pp. 579–587, 2012.

[65] Z. Trad, A. Barkaoui, and M. Chafra, "A three dimensional finite element analysis of mechanical stresses in the human knee joint: Problem of cartilage destruction," in *Journal of Biomimetics, Biomaterials and Biomedical Engineering*, vol. 32, pp. 29–39, Trans Tech Publ, 2017.

[66] L. Li, L. Yang, K. Zhang, L. Zhu, X. Wang, and Q. Jiang, "Three-dimensional finite-element analysis of aggravating medial meniscus tears on knee osteoarthritis," *Journal of orthopaedic translation*, vol. 20, pp. 47–55, 2020.

[67] E. Peña, B. Calvo, M. A. Martínez, and M. Doblaré, "Effect of the size and location of osteochondral defects in degenerative arthritis. a finite element simulation," *Computers in biology and medicine*, vol. 37, no. 3, pp. 376–387, 2007.

[68] R. G. Nagassa, P. G. McMenamin, J. W. Adams, M. R. Quayle, and J. V. Rosenfeld, "Advanced 3d printed model of middle cerebral artery aneurysms for neurosurgery simulation," *3D printing in medicine*, vol. 5, pp. 1–12, 2019.

[69] B. Utela, D. Storti, R. Anderson, and M. Ganter, "A review of process development steps for new material systems in three dimensional printing (3dp)," *Journal of Manufacturing Processes*, vol. 10, no. 2, pp. 96–104, 2008.

[70] P. Gargiulo, Í. Árnadóttir, M. Gíslason, K. Edmunds, and I. Ólafsson, "New directions in 3d medical modeling: 3d-printing anatomy and functions in neurosurgical planning," *Journal of healthcare engineering*, vol. 2017, 2017.

[71] K. Tappa and U. Jammalamadaka, "Novel biomaterials used in medical 3d printing techniques," *Journal of functional biomaterials*, vol. 9, no. 1, p. 17, 2018.

[72] J.-Y. Park, H.-Y. Kim, J.-H. Kim, J.-H. Kim, and W.-C. Kim, "Comparison of prosthetic models produced by traditional and additive manufacturing methods," *The journal of advanced prosthodontics*, vol. 7, no. 4, pp. 294–302, 2015.

[73] P. Honigmann, N. Sharma, B. Okolo, U. Popp, B. Msallem, and F. M. Thieringer, "Patient-specific surgical implants made of 3d printed peek: material, technology, and scope of surgical application," *BioMed research international*, vol. 2018, 2018.

[74] C. L. Ventola, "Medical applications for 3d printing: current and projected uses," *Pharmacy and Therapeutics*, vol. 39, no. 10, p. 704, 2014.

[75] C. M. González-Henríquez, M. A. Sarabia-Vallejos, and J. Rodriguez-Hernandez, "Polymers for additive manufacturing and 4d-printing: Materials, methodologies, and biomedical applications," *Progress in Polymer Science*, vol. 94, pp. 57–116, 2019.

[76] D. Hoang, D. Perrault, M. Stevanovic, and A. Ghiassi, "Surgical applications of three-dimensional printing: a review of the current literature & how to get started," *Annals of Translational Medicine*, vol. 4, no. 23, 2016.

[77] L. Severseike, V. Lee, T. Brandon, C. Bakken, and V. Bhatia, "Polyjet 3d printing of tissue-mimicking materials: how well can 3d printed synthetic myocardium replicate mechanical properties of organic myocardium?," *BioRxiv*, p. 825794, 2019.

[78] A. J. Sparks, C. M. Smith, A. B. Allman, J. L. Senko, K. M. Meess, R. W. Ducharme, M. E. Springer, M. Waqas, and A. H. Siddiqui, "Compliant vascular models 3d printed with the stratasys j750: a direct characterization of model distensibility using intravascular ultrasound," *3D Printing in Medicine*, vol. 7, no. 1, pp. 1–11, 2021.